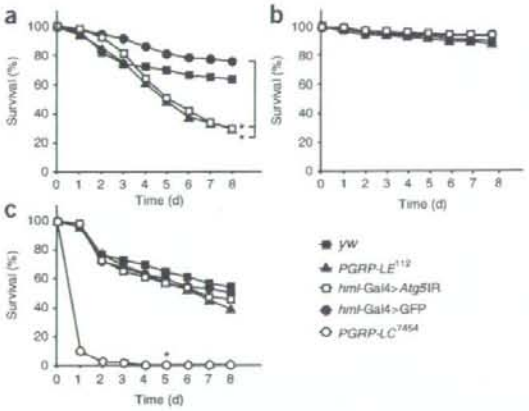

Figure 3 Autophagy is crucial for host survival after *L. monocytogenes* infection. Survival of *yw* flies, *PGRP-LE*^{112} flies, flies treated with *Atg5*-directed RNAi (*hml*-Gal4 > *Atg5*IR) and control flies carrying *hml*-Gal4 (*hml*-Gal4 > GFP), after injection of wild-type *L. monocytogenes* (**a**), Δ*hly* *L. monocytogenes* (**b**) or *E. carotovora* (**c**) into adult flies. *, $P < 0.01$ (Wilcoxon-Mann-Whitney test): $P = 0.0024$, *Atg5*-directed RNAi versus control (**a**), $P = 0.0007$, *PGRP-LE*^{112} versus control (**a**); $P = 0.0055$, *PGRP-LC*^{7454} versus *yw* (**c**). Data represent the average of four independent experiments.

(**Supplementary Fig. 4** online); thus, we compared *L. monocytogenes* infection in S2 cells with that in S2 cells stably transfected with a metallothionein promoter–PGRP-LE expression plasmid[5]. Incubation for 1.5 h with wild-type *L. monocytogenes*, followed by additional incubation for 6 h in medium containing gentamicin and 100 μM $CuSO_4$ to induce PGRP-LE, decreased the number of bacteria in the cells to numbers similar to those noted after infection with the Δ*hly* strain (**Fig. 4a**). *Atg5* knockdown by RNAi in S2 cells expressing PGRP-LE (**Supplementary Fig. 4b**) restored the number of bacteria to that in S2 cells (**Fig. 4a**). Infection of S2 cells expressing PGRP-LE with wild-type *L. monocytogenes* induced AMP expression in a PGRP-LE-dependent way (**Supplementary Fig. 5a** online). This induction was totally dependent on *imd*, which encodes a key factor of the Imd pathway (**Supplementary Fig. 5b**). In contrast to AMP induction, PGRP-LE-mediated suppression of bacterial growth was not affected by knockdown of *Relish* or *imd* (**Fig. 4a** and data not shown). PGRP-LE-mediated suppression of bacterial growth was also not affected by knockdown of *Dif* and *dl* (**Fig. 4a**). However, AMP induction was not affected by *Atg5* knockdown (**Supplementary Fig. 5b**), which suggests that the autophagy pathway is not essential for AMP induction in *L. monocytogenes* infection. Knockdown of the expression of *Relish*, *Dif* and *dl*, or *Atg5* had no effect on the number of Δ*hly* strain bacteria in either S2 cells or S2 cells expressing PGRP-LE (**Fig. 4a**), which suggests that the products of these genes are not involved in phagocytic entry of the bacteria. These results suggest that the autophagy pathway but not NF-κB transcription factors (Relish, Dif or dorsal) is required for PGRP-LE-mediated suppression of intracellular *L. monocytogenes* growth. Consistent with the results suggesting the importance of the autophagy pathway in the PGRP-LE-mediated suppression of intracellular listeria growth, a time-course evaluation of the intracellular growth of the bacteria in S2 cells expressing PGRP-LE showed a decrease in the number of intracellular wild-type but not Δ*hly* *L. monocytogenes* at 2.5 h after infection (0.5 h of infection plus 2 h with gentamicin). At later time points, the bacteria remained at low numbers in the S2 cells expressing PGRP-LE but multiplied robustly in S2 cells that did not express PGRP-LE (**Supplementary Fig. 6** online).

As noted above, PGRP-LE functions as an intracellular receptor by detecting peptidoglycan fragments[5] and is essential for suppressing intracellular bacterial growth. To test the possibility that PGRP-LE detects bacteria that invade host cell cytoplasm, we infected S2 cells expressing yellow fluorescent protein (YFP)-tagged PGRP-LE[5] with wild-type or Δ*hly* strain *L. monocytogenes* and assayed them by confocal fluorescence microscopy (**Fig. 4b,c**). With no bacterial infection, YFP-tagged PGRP-LE was dispersed throughout the cytoplasm[5]. After infection with wild-type bacteria, however, YFP-tagged PGRP-LE accumulated around the bacteria (**Fig. 4b**); in contrast, infection with the Δ*hly* strain, which cannot enter the cytoplasm, did not result in the accumulation of YFP-tagged PGRP-LE around bacteria (**Fig. 4c**). These results suggest that PGRP-LE directly detects invading *L. monocytogenes* after it enters the cytoplasm.

Autophagy induction by PGRP-LE

The data reported above suggested that intracellular PGRP-LE is responsible for detecting invading *L. monocytogenes* and for inducing autophagy. To test that possibility, we determined whether *L. monocytogenes* invading the cell cytoplasm was surrounded by autophagosomes in a PGRP-LE-dependent way. We expressed a fusion

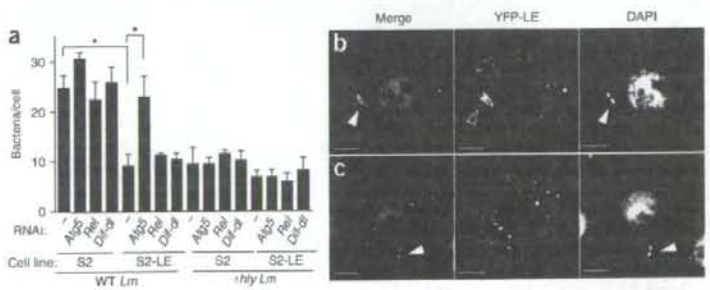

Figure 4 Autophagy, but not the IMD or Toll pathway, is crucial for PGRP-LE-mediated suppression of the intracellular growth of *L. monocytogenes* in S2 cells. (**a**) Growth of *L. monocytogenes* in S2 cells (S2) or S2 cells expressing PGRP-LE (S2-LE) transfected with double-stranded RNA (RNAi) specific for *Atg5*, *Rel* or *Dif* and *dl* (*Dif-dl*) and infected for 1.5 h with wild-type or Δ*hly* *L. monocytogenes*, followed by 6 h of incubation in medium containing $CuSO_4$ and gentamicin, quantified by plate assay of colony-forming units. *, $P < 0.001$ (*t*-test). Data are representative of two independent experiments (error bars, s.d.). (**b,c**) Fluorescence confocal microscopy of the localization of PGRP-LE together with wild-type *L. monocytogenes* in S2 cells engineered to express YFP–PGRP-LE (YFP-LE) and infected for 0.5 h with wild-type *L. monocytogenes* (**b**) or Δ*hly* *L. monocytogenes* (**c**), followed by 1 h of incubation in gentamicin-containing medium, then DAPI staining. Merge, YFP–PGRP-LE (green) and DAPI (magenta). Filled arrowheads indicate *L. monocytogenes*; open arrowhead indicates accumulation of YFP–PGRP-LE around the bacteria. Scale bars, 5 μm. Data are representative of three experiments.

protein of LC3 and green fluorescent protein (GFP)[33] under the control of the promoter of a gene encoding actin in S2 cells and in S2 cells expressing PGRP-LE and examined the distribution of GFP-LC3 by confocal fluorescence microscopy (**Fig. 5a–i**). GFP-LC3 is an autophagosome-specific membrane marker detected in dot- or ring-shaped structures when autophagosomes are formed in mammalian cell cytoplasm[13,14,33] and in drosophila fat body cells[27]. In contrast to a published report showing that TLR4-dependent induction of autophagy by lipopolysaccharide treatment in a mouse macrophage cell line is maximal 12–16 h after lipopolysaccharide stimulation[19], we found dot- or ring-shaped GFP-LC3 signals in S2 cells expressing PGRP-LE after only 1.5 h of incubation (0.5 h of initial incubation plus an additional 1 h in the presence of gentamicin) with wild-type *L. monocytogenes* (**Fig. 5a,c**). The number of GFP-LC3 dots in cells infected with the Δ*hly* strain was near the background number (**Fig. 5a**). In S2 cells, in which no detectable PGRP-LE is expressed, infection with wild-type *L. monocytogenes* did not increase the formation of GFP-LC3 dots (**Fig. 5a**). These results suggest that PGRP-LE is essential for the formation of GFP-LC3 dots caused by invasion of the cell cytoplasm with wild-type *L. monocytogenes*. Treatment of cells with rapamycin, an inhibitor of autophage-inhibitory factor TOR[29], induced a similar frequency of GFP-LC3 dots in S2 cells and in S2 cells expressing PGRP-LE (**Fig. 5a**), which suggested that the formation of dot- or ring-shaped GFP-LC3 itself was not affected by the lack of PGRP-LE expression. In S2 cells expressing PGRP-LE and infected with wild-type *L. monocytogenes*, one or many bacteria were often surrounded by ring-shaped GFP-LC3 dots (**Fig. 5b,c**). We detected colocalization of wild-type bacteria and GFP-LC3 dots in S2 cells expressing PGRP-LE after 0.5 h incubation with bacteria, and the frequency of the colocalization after 1.5 h of incubation (0.5 h incubation with bacteria plus 1 h in the presence of gentamicin) was 57.7% ± 5.3%, significantly higher than that in S2 cells infected with wild-type bacteria (7.9% ± 6.9%; **Fig. 5b**).

During the autophagic processes, cytosolic LC3 (LC3-I) is conjugated on its carboxyl terminus with phosphatidylethanolamine, and the lipidated LC3 (LC3-II) localizes to the autophagic membrane[34]. Therefore, the amount of LC3-II correlates with the number of autophagosomes. After infection, GFP–LC3-II increased considerably in S2 cells expressing PGRP-LE, whereas there was no change in GFP–LC3-II in infected parental S2 cells that did not express PGRP-LE (**Fig. 5d**). Rapamycin treatment induced an increase in GFP–LC3-II in both cell types (**Fig. 5d**). These observations suggest that PGRP-LE is

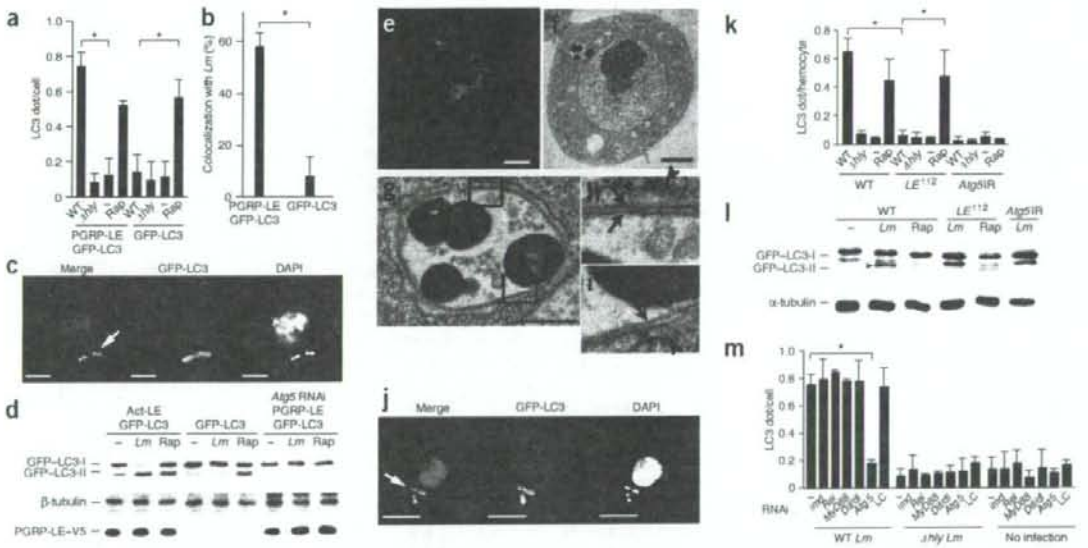

Figure 5 PGRP-LE mediates autophagosome formation in S2 cells and hemocytes. (**a**) Dot- or ring-shaped GFP-LC3 (LC3 dot) signals in S2 cells expressing both PGRP-LE and GFP-LC3 under the control of an actin promoter (PGRP-LE GFP-LC3) or GFP-LC3 alone (GFP-LC3) after infection with wild-type or Δ*hly L. monocytogenes* or after 1.5 h of incubation with 5 μM rapamycin (rap). –, no infection. (**b**) Colocalization of GFP-LC3 dots and wild-type *L. monocytogenes* in S2 cells, quantified by confocal microscopy. (**c**) Confocal microscopy of S2 cells expressing PGRP-LE and GFP-LC3 (green) infected with wild-type *L. monocytogenes* and stained with DAPI (magenta). Arrow indicates colocalization of GFP-LC3 and *L. monocytogenes*. (**d**) Immunoblot analysis of lysates of S2 cells left untreated (–) or infected with wild-type *L. monocytogenes* or treated with 5 μM rapamycin. (**e–i**) Ultrastructural analysis of S2 cells expressing PGRP-LE and GFP-LC3 and infected with wild-type *L. monocytogenes*. (**e,f**) Fluorescence microscopy (**e**) and electron microscopy (**f**) of cells expressing GFP-LC3 (green) and stained with DAPI (magenta). (**g**) Enlargement of a bacteria-containing vacuole from **f**. (**h,i**) Enlargement of the fields outlined in **g**. Arrows indicate double-membrane structure that surrounds the bacteria; arrowheads indicate an endoplasmic reticulum–like membrane. (**j**) Confocal microscopy of hemocytes infected with wild-type *L. monocytogenes*. Green, GFP-LC3; magenta, DAPI. Arrow indicates colocalization of GFP-LC3 and *L. monocytogenes*. (**k**) Dot- or ring-shaped GFP-LC3 signals in *ex vivo*–cultured hemocytes expressing GFP-LC3 (infection and treatment, horizontal axis). (**l**) Immunoblot analysis of lysates of hemocytes from third instar larvae cultured *ex vivo* and infected with *L. monocytogenes* or treated with rapamycin. Arrowhead indicates processed form of GFP-LC3. (**m**) GFP-LC3 dots in S2 cells expressing PGRP-LE and GFP-LC3 and treated with RNAi (below graph) and infected for 0.5 h with *L. monocytogenes* then incubated for 1 h in gentamicin-containing medium; dots quantified by confocal microscopy. Scale bars, 5 μm (**c,j**), 1 μm (**e,f**) or 500 nm (**g**). *, $P < 0.001$ (*t*-test). Data are representative of three (**a,k,m**), two (**b,e–i**), six (**c**), four (**d**) or five (**j,l**) experiments (error bars, s.d. of triplicate measurements (**a,b,l**) or at least triplicate measurements (**m**)).

not essential for autophagosome formation itself but that autophagosome formation is induced through PGRP-LE when *L. monocytogenes* invades the cytoplasm. As expected, *Atg5* knockdown prevented the conversion of LC3-I to LC3-II after bacterial infection or rapamycin treatment (**Fig. 5d**).

Next we investigated whether the structures associated with GFP-LC3–containing structures that surrounded *L. monocytogenes* had the typical characteristics of autophagosomes. At 1 h after infection (0.5 h of initial incubation plus an additional 0.5 h in the presence of gentamicin), we examined GFP-LC3 dots in S2 cells expressing PGRP-LE and GFP-LC3 by fluorescence microscopy (**Fig. 5e**); we also studied the same fields by electron microscopy (**Fig. 5f–i**). We noted double-membrane structures engulfing the bacteria (**Fig. 5g–i**), which suggested that recognition of *L. monocytogenes* by PGRP-LE in the cytoplasm induces conventional autophagy around the bacteria.

We then determined whether endogenously expressed PGRP-LE is essential for inducing autophagy after infection of hemocytes by *L. monocytogenes*. We expressed GFP-LC3 with heat-shock–Gal4 in the third instar larvae and cultured hemocytes from the larvae *ex vivo* with *L. monocytogenes*. After 1 h of incubation with wild-type *L. monocytogenes* followed by an additional 1 h of incubation in gentamicin-containing medium, we found GFP-LC3 dots in *L. monocytogenes*–infected wild-type hemocytes, and confocal microscopy showed that infected *L. monocytogenes* were surrounded by structures containing GFP-LC3 (**Fig. 5j,k**). In contrast, the frequency of the formation of GFP-LC3 dots was similar in uninfected and infected *PGRP-LE*^{112} hemocytes (**Fig. 5k**). This result was not due to lower phagocytic activity in *PGRP-LE*^{112} hemocytes, because similar numbers of Δ*hly L. monocytogenes* infected *PGRP-LE*^{112} and wild-type hemocytes (**Fig. 2b**). Similarly, this result was not due to a generalized defect in autophagosome formation in *PGRP-LE*^{112} hemocytes, as the frequency and morphology of the GFP-LC3 dots induced by rapamycin treatment was similar in *PGRP-LE*^{112} and wild-type hemocytes (**Fig. 5k** and **Supplementary Fig. 7** online). Targeting of *Atg5* by a Gal4-dependent RNAi transgene greatly decreased the number of GFP-LC3 dots per infected cell to that in uninfected cells (**Fig. 5k**). We rarely detected GFP-LC3 dots in Δ*hly* strain–infected hemocytes (**Fig. 5k**). Together, these data indicate that *L. monocytogenes* invasion of the cytoplasm induces autophagy in a way dependent on endogenously expressed functional PGRP-LE.

We confirmed the PGRP-LE-dependent induction of autophagy in hemocytes by immunoblot analysis that showed the modification of GFP-LC3. We incubated wild-type and *PGRP-LE*^{112} hemocytes expressing GFP-LC3, or hemocytes expressing an RNAi transgene targeting *Atg5*, *ex vivo* for 0.5 h with wild-type *L. monocytogenes*, followed by additional incubation for 2 h in gentamicin-containing medium. We then analyzed the modification of GFP-LC3 by immunoblot with antibody to GFP (anti-GFP). *L. monocytogenes* infection or rapamycin treatment of wild-type hemocytes enhanced the intensity of the processed form of GFP-LC3, whereas infection had no effect on GFP-LC3 processing in the *PGRP-LE*^{112} mutant or *Atg5* RNAi hemocytes (**Fig. 5l**). These results indicate that PGRP-LE is required for the induction of autophagy in response to *L. monocytogenes* infection.

PGRP-LE-mediated induction of AMP in response to *L. monocytogenes* infection in S2 cells was dependent on the IMD pathway (**Supplementary Fig. 5**). PGRP-LE-mediated suppression of intracellular bacterial growth in S2 cells and hemocytes, however, was not dependent on the IMD and Toll pathways. We therefore determined whether PGRP-LE-mediated autophagosome formation was dependent on the IMD and/or Toll signaling pathways. We quantified GFP-LC3 dots per cell in wild-type *L. monocytogenes*–infected S2 cells expressing both PGRP-LE and GFP-LC3. Knockdown of *imd*, *Relish*, *MyD88*, or both *Dif* and *dl* by RNAi in wild-type *L. monocytogenes*–infected S2 cells expressing PGRP-LE and GFP-LC3 did not affect the formation of GFP-LC3 dots, but *Atg5* knockdown decreased the number of LC3 dots per cell (**Fig. 5m**). Knockdown of *PGRP-LC* also did not affect the formation of GFP-LC3 dots (**Fig. 5m**). These results suggest that the PGRP-LE-mediated autophagosome formation is independent of IMD and Toll pathways, consistent with other data indicating that PGRP-LE-mediated suppression of intracellular bacterial growth did not involve with these pathways (**Fig. 4a**).

Autophagy induced by DAP-type PGN

PGRP-LE recognizes TCT and DAP-containing PGN[4,5]. We next determined whether TCT and PGN induced autophagy in the cell cytoplasm. We used a calcium phosphate method to transfect highly purified TCT[35], highly purified DAP-type PGN or highly purified lysine-type PGN into S2 cells expressing PGRP-LE and GFP-LC3 and quantified GFP-LC3 dots after 2 h of incubation. TCT, DAP-type PGN or lysine-type PGN increased the number of GFP-LC3 dots per cell to a frequency similar to that in *L. monocytogenes*–infected cells (**Fig. 6a**). In contrast, lysine-type PGN but not TCT or DAP-type PGN induced an increase in the number of GFP-LC3 dots in S2 cells lacking PGRP-LE (**Fig. 6a**). We obtained similar results with chemically synthesized TCT (data not shown). Transfection of either of two synthetic desmuramylpeptides (peptidoglycan fragments containing DAP), FK156 (ref. 36) or its derivative, FK565, did not increase the number of GFP-LC3 dots in S2 cells expressing PGRP-LE (data not shown). Correlative fluorescence microscopy–electron microscopy showed that the TCT-induced GFP-LC3–expressing dots had double-membrane structures typical of autophagosomes (**Supplementary Fig. 8a,b** online). These results suggest that autophagy induction mediated by TCT and DAP-type PGN is dependent on PGRP-LE but that autophagy induction mediated by lysine-type PGN is not. We also examined the formation of GFP-LC3 dots in response to TCT, DAP-type PGN or lysine-type PGN in hemocytes cultured *ex vivo*, although the precise mechanism of cytoplasmic delivery of PGN in hemocytes is not clear. The formation of GFP-LC3 dots dependent on TCT and DAP-type PGN was suppressed in *PGRP-LE*^{112} mutant hemocytes relative to that of their wild-type counterparts, but lysine-type PGN–dependent formation of GFP-LC3 dots was not affected in *PGRP-LE*^{112}

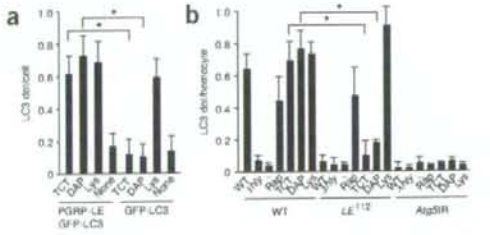

Figure 6 PGRP-LE is responsible for autophagy induced by TCT and DAP-type PGN. (**a**) GFP-LC3 dots in S2 cells expressing GFP-LC3 alone or PGRP-LE and GFP-LC3, treated for 2 h with TCT (100 nM), highly purified DAP-type PGN from *L. plantarum* (DAP; 100 μg/ml) or lysine-type PGN from *S. epidermidis* (Lys). (**b**) Dot- or ring-shaped GFP-LC3 signals in hemocytes after infection with wild-type or Δ*hly L. monocytogenes* or treatment with rapamycin (5 μM) or with TCT, DAP-type PGN or lysine-type PGN. *, $P < 0.001$ (*t*-test). Data are representative of two independent experiments (error bars, s.d.).

mutant hemocytes (**Fig. 6b** and **Supplementary Fig. 8c–h**). These results suggest that PGRP-LE is crucial for the induction of autophagosome formation in response to TCT and DAP-type PGN but not in response to lysine-type PGN. Together, these findings indicate that PGRP-LE probably recognizes DAP-type PGN of *L. monocytogenes* to induce autophagy.

DISCUSSION

Evidence has indicated the importance of autophagy as a defense against intracellular pathogens, and the mechanism underlying the induction of autophagy during pathogen infection is a central issue. The results of our study here have demonstrated that PGRP-LE, through its ability to induce autophagy and prevent intracellular bacterial growth, is essential in drosophila for resistance against *L. monocytogenes*. Our findings have indicated that the induction of autophagy, as an innate defense mechanism targeting intracellular pathogens, is activated by intracellular microbial sensors. In mammalian cells, the Nod-like receptors (or other intracellular microbial receptors) may sense bacterial invasion of the cytoplasm and induce autophagy in response to cytoplasm-invading bacterial infection. In fact, autophagy induction during infection of mouse embryonic fibroblast cells with *L. monocytogenes* requires the expression of listeriolysin O[28], which suggests that the sensing of *L. monocytogenes* in mammalian cells also occurs in the cytoplasm.

In primary hemocytes and S2 cells, both DAP-type and lysine-type PGN induced autophagy, although PGRP-LE was responsible only for the autophagy induction stimulated by DAP-type PGN. These results suggest that other cytoplasmic sensors detect invading bacteria with cell walls containing lysine-type PGN. In mammals, autophagy has also been linked to resistance to parasites, such as *T. gondii*, and viruses[12]. Although the fundamental mechanisms linking these pathogens with the autophagy machinery might be similar to that used in bacterial infection, it is likely that the host cells use distinct sensors to induce autophagy in response to each type of pathogen.

Although the molecular mechanisms and signaling pathways leading to starvation-induced autophagy are well studied, the signaling pathways that induce autophagy after pathogen infection are just beginning to be clarified. In contrast to AMP induction, PGRP-LE-mediated induction of autophagy was independent of the Toll and IMD pathways. However, autophagy induced by lipopolysaccharide through TLR4 signaling dependent on the adaptor TRIF has been shown to overcome an *M. tuberculosis*–mediated phagosome block and promote its localization together with autophagosomes[19]. PGRP-LE has a RHIM-like motif that is similar to the receptor-interacting protein homotypic interaction motif present in TRIF and the signaling mediator RIP1 (ref. 5). This motif is required for the interaction between TRAF and RIP1 and for TRIF- and TLR3-induced NF-κB activation[37,38]. It is possible that an unidentified factor with a RHIM-like motif interacts with PGRP-LE to activate the signaling pathway to induce autophagy. Autophagy has been shown to be essential in the defense against several kinds of pathogens in cultured cells[13–17]. Thus, our report opens the door to investigation of the connection between intracellular pattern-recognition receptors and autophagy as an immune response, as well as the signaling pathways involved in both insects and mammals.

METHODS

Fly strains. Stocks were raised on a standard cornmeal-yeast agar medium at 25 °C. The following strains have been described elsewhere: *ywPGRP-LE*^{112} (*PGRP-LE*^{112})[5], *w;;PGRP-LC*^{7454} (*PGRP-LC*^{7454})[39], *Relish*^{E20} (ref. 3), *w;;Atg1*$^{\Delta 3D}$ (*Atg1*$^{\Delta 3D}$)[26], *w;;hml*-Gal4 (*hml*-Gal4)[25], *w;;cg*-Gal4 (*cg*-Gal4)[30], *w*;UAS-PGRP-LE (PGRP-LE)[4], *yw*UAS-Atg5 IR (*Atg5*IR)[26], *yw;;*UAS-Atg1^{6B} (ref. 30) and *w*;UAS-GFP-LC3 (GFP-LC3)[27].

Survival experiments. Flies were infected with bacteria through the injection of approximately 70 nl per fly of a dilution of cultured bacterial strains (1/100,000 dilution of an *L. monocytogenes* suspension or *E. carotovora* suspension; absorbance of 1.0 at 600 nm), which resulted in the injection of approximately 10 bacteria per fly. All survival experiments used 30 flies for each genotype and were done at 28 °C for *L. monocytogenes* injection or 25 °C for *E. carotovora* injection. Surviving flies were transferred daily into fresh vials.

***L. monocytogenes* infection of hemocytes cultured *ex vivo*.** Third instar larvae mounted on concanavalin A–treated glass slides were dissected in Schneider's drosophila medium containing 10% (vol/vol) FBS. After a few minutes of incubation to allow the hemocytes to attach to the glass slide, the medium was replaced with new medium and a suspension of *L. monocytogenes* grown to mid-log phase was added to the culture (approximately 20 bacteria per cell), followed by 1 h of incubation at 28 °C. Cells were washed and further incubated for various times at 28 °C in Schneider's drosophila medium containing 10% (vol/vol) FBS and gentamicin (10 μg/ml). Cells were then fixed with 2% (wt/vol) paraformaldehyde for immunohistochemical analysis. For the induction of GFP-LC3, third instar larvae were treated to heat shock (20 min at 37 °C) at 12 h before hemocyte isolation.

Bacterial strains. The following *L. monocytogenes* strains were used: 10403S (wild-type strain), DP-L2161 (Δ*hly* strain)[31], DH-L1039 (GFP-expressing wild-type strain) and DH-L1137 (GFP-expressing Δ*hly* strain)[32]. *E. carotovora* carotovora strain 15 was used in survival experiments.

PGN. DAP-type and lysine-type PGN were highly purified from *Lactobacillus plantarum* (American Type Culture Collection 8014) and *Staphylococcus epidermidis* (American Type Culture Collection 155), respectively, according to a published method[40]. Purity was confirmed by amino acid analysis. Highly purified TCT has been described[35]. Chemically synthesized TCT was prepared with an orthogonally protected *meso*-DAP containing a tetrapeptide (L-Ala-γ-D-Glu(OBn)-*meso*-DAP(*N*-Z, OBn)-D-Ala(OBn)) and a disaccharide (4,6-*O*-benzylidene-3-*O*-benzyl-GlcNAc-(β1-4)-MurNAc(anh)). After condensation of the disaccharide and the tetrapeptide with water-soluble carbodiimide hydrochloride (1-ethyl-3-(3-dimethylaminopropyl)carbodiimide hydrochloride), 1-hydroxybenzotriazole, triethylamine, in *N,N*-dimethyl formamide, deprotection of all the protecting groups by hydrogenation (H_2 (20 kg/cm^2) and $Pd(OH)_2$ in tetrahydrofuran) resulted in TCT. The molecular weight of TCT was confirmed by an electrospray ionization–time-of-flight–mass spectrometry (negative) mass/charge ratio of 920.4 [M-H]; high-resolution electrospray ionization–time-of-flight–mass spectrometry (positive) mass/charge ratio of 922.3898 $[M+H]^+$ (theoretical value for $C_{29}H_{48}N_6O_{16}$ (TCT); 922.3893, $[M+H]^+$). FK156 (D-lactyl-L-Ala-γ-D-Glu-*meso*-DAP-Gly)[36] and its derivative, FK565 (haptanoyl-γ-D-Glu-*meso*-DAP-D-Ala), were supplied by Astellas Pharmaceutical (formerly Fujisawa and Yamanouchi).

RNAi in S2 cells. The double-stranded RNA used in the RNAi experiments was synthesized as described[5]. Templates for double-stranded *Atg5* RNA were amplified with the primers 5′-TAATACGACTCACTATAGGGCAAATAAGGAA CATGGCC-3′ and 5′-TAATACGACTCACTATAGGGTCAGGCAGGACATG TAG-3′. Double-stranded RNA was transfected into S2 cells as described[5].

***L. monocytogenes* infection of S2 cells and intracellular bacteria counts.** Cultures (1 × 10^6 cells/ml) were incubated for 18 h and 50 nM water-soluble cholesterol was added to the culture as described[30]. After 30 min of incubation, a suspension of *L. monocytogenes* (approximately 20 bacteria per cell unless stated otherwise) was added and the cells were incubated for 1.5 h at 28 °C for infection with 20 bacteria per cell. Cells were then washed with PBS and were incubated for 6 h in Schneider's drosophila medium containing $CuSO_4$ (100 μM) and gentamicin (10 μg/ml). After being washed with PBS, cells were dispersed in water to release bacteria from the cytoplasm of the S2 cells. Samples were then plated on brain-heart infusion plates for measurement of colony-forming units.

Immunohistochemistry. Fixed hemocytes or S2 cells were washed with PBS and were stained for 1 h with anti-GFP (598; Medical & Biological Laboratories) in PBS containing 1% (wt/vol) BSA and 0.1% (vol/vol) Triton X-100, followed by 1 h with fluorescein isothiocyanate–labeled anti–rabbit immunoglobulin G (F-2765; Molecular Probes) and rhodamine-labeled phalloidin (R-415; Molecular Probes) where required, then 10 min of staining with DAPI (Sigma). For the detection of GFP-LC3 in hemocytes, flies of the following genotypes were analyzed: *w*; UAS-GFP-LC3/UAS-Gal4; heat-shock–Gal4/+, *PGRPLE*^{112}; UAS-GFP-LC3/UAS-Gal4; heat-shock–Gal4/+,UAS-*Atg5IR*/+; UAS-GFP-LC3/UAS-Gal4; heat-shock–Gal4/+.

Immunoblot analysis. S2 cells were infected for 0.5 h at 28 °C with wild-type *L. monocytogenes* (approximately 500 bacteria per cell) and were further incubated for 1 h at 28 °C in gentamicin-containing medium. Hemocytes cultured *ex vivo* were infected for 1 h at 28 °C with wild-type *L. monocytogenes* (approximately 200 bacteria per cell), were washed with PBS and were further incubated for 2 h at 28 °C in gentamicin-containing medium. For immunoblot analysis, cells were washed with PBS and lysed with buffer containing 50 mM Tris-HCl, 2% (wt/vol) SDS, 10% (vol/vol) glycerol and 100 mM β-mercaptoethanol. Lysates from the same number of cells were separated by 10% SDS-PAGE and transferred to polyvinylidene membranes and then analyzed by immunoblot with anti-GFP (598; Medical & Biological Laboratories), anti-α-tubulin (H-300; Santa Cruz Biotechnology), anti-β-tubulin (E7; Hybridoma Bank) or anti-V5 (tag; 46-0705; Invitrogen). Blots were visualized with the ECL-Western Blotting Analysis system (GE Healthcare).

Correlative fluorescence microscopy–electron microscopy. This correlative microscopy allows analysis of individual cells both in an overview with fluorescence microscopy and in a detailed subcellular structure view with electron microscopy. For observation with this microscopy, S2 cells cultured on glass-bottomed dishes (MatTek) were fixed for 2 h with 2% (wt/vol) paraformaldehyde and 2.5% (vol/vol) glutaraldehyde in 0.1 M sodium cacodylate, pH 7.4, and then were examined with a confocal laser-scanning microscope. The same specimens were further incubated overnight at 4 °C in the same buffer. After being washed three times with a buffer of 0.1 M sodium cacodylate, pH 7.4, containing 7% (wt/vol) sucrose, samples were post-fixed for 1 h with 1% (wt/vol) osmium tetroxide and 0.5% (wt/vol) potassium ferrocyanide in the same buffer, then were washed with distilled water three times, dehydrated in ethanol and embedded in Epon812 (TAAB Laboratories Equipment). Ultrathin cell sections (70 nm in thickness) were stained with saturated uranyl acetate and Reynolds lead citrate solution. Electron micrographs were obtained with a JEM-1011 transmission electron microscope (JEOL).

Note: Supplementary information is available on the Nature Immunology website.

ACKNOWLEDGMENTS

We thank D.A. Portnoy (University of California, Berkeley) and D.E. Higgins (Harvard Medical School) for *L. monocytogenes* strains; L.W. Cheng (University of California, Berkeley) for the S2 cell *L. monocytogenes* infection protocol; T.P. Neufeld (University of Minnesota) for *Atg1*$^{\Delta 3D}$, *Atg5*IR, *Atg1* and GFP-LC3; D. Hultmark (Umeå University) for *Relish*^{E20}; K. Anderson (Cornell University) for *PGRP-LC*$^{\Delta 5}$^{4}; A. Goto (Tohoku University) for *hml*-Gal4; the Bloomington Stock Center, Drosophila Genetic Resource Center at the Kyoto Institute of Technology and the Genetic Strain Research Center of National Institute of Genetics for fly stocks; and S. Iwanaga, M. Mitsuyama, A. Yamamoto and S. Natori for discussions. Supported by Grants-in-Aid for Scientific Research from the Ministry of Education, Culture, Sports, Science and Technology of Japan; the Japan Society for the Promotion of Science; the Program for the Promotion of Basic Research Activities for Innovative Biosciences; the National Institutes of Health (AI60025 and AI074958 to N.S.; AI074958); and the Naito Foundation.

Published online at http://www.nature.com/natureimmunology/
Reprints and permissions information is available online at http://npg.nature.com/reprintsandpermissions/

1. Lemaitre, B. & Hoffmann, J. The host defense of *Drosophila melanogaster*. *Annu. Rev. Immunol.* **25**, 697–743 (2007).
2. Ferrandon, D., Imler, J.-L., Hetru, C. & Hoffmann, J.A. The *Drosophila* systemic immune response: sensing and signaling during bacterial and fungal infections. *Nat. Rev. Immunol.* **7**, 862–874 (2007).
3. Takehana, A. *et al.* Peptidoglycan recognition protein (PGRP)-LE and PGRP-LC act synergistically in *Drosophila* immunity. *EMBO J.* **23**, 4690–4700 (2004).
4. Takehana, A. *et al.* Overexpression of a pattern-recognition receptor, peptidoglycan-recognition protein-LE, activates imd/relish-mediated antibacterial defense and the prophenoloxidase cascade in *Drosophila* larvae. *Proc. Natl. Acad. Sci. USA* **99**, 13705–13710 (2002).
5. Kaneko, T. *et al.* PGRP-LC and PGRP-LE have essential yet distinct functions in the drosophila immune response to monomeric DAP-type peptidoglycan. *Nat. Immunol.* **7**, 715–723 (2006).
6. Lemaitre, B., Reichhart, J.-M. & Hoffmann, J.A. *Drosophila* host defense: Differential induction of antimicrobial peptide genes after infection by various classes of microorganisms. *Proc. Natl. Acad. Sci. USA* **94**, 14614–14619 (1997).
7. Kanneganti, T.-D., Lamkanfi, M. & Núñez, G. Intracellular NOD-like receptor in host defense and disease. *Immunity* **27**, 549–559 (2007).
8. Chaput, C. & Boneca, I.G. Peptidoglycan detection by mammals and flies. *Microbes Infect.* **9**, 637–647 (2007).
9. Delbridge, L.M. & O'Riordan, M.X.D. Innate recognition of intracellular bacteria. *Curr. Opin. Immunol.* **19**, 10–16 (2007).
10. Hsu, Y.M. *et al.* The adaptor protein CARD9 is required for innate immune responses to intracellular pathogens. *Nat. Immunol.* **8**, 198–205 (2007).
11. Mizushima, N. Autophagy: process and function. *Genes Dev.* **21**, 2861–2873 (2007).
12. Levine, B. & Deretic, V. Unveiling the roles of autophagy in innate and adaptive immunity. *Nat. Rev. Immunol.* **7**, 767–777 (2007).
13. Nakagawa, I. *et al.* Autophagy defends cells against invading Group A *Streptococcus*. *Science* **306**, 1037–1040 (2004).
14. Gutierrez, M.G. *et al.* Autophagy is a defense mechanism inhibiting BCG and *Mycobacterium tuberculosis* survival in infected macrophages. *Cell* **119**, 753–766 (2004).
15. Ogawa, M. *et al.* Escape of intracellular *Shigella* from autophagy. *Science* **307**, 727–731 (2005).
16. Ling, Y.M. *et al.* Vacuolar and plasma membrane stripping and autophagic elimination of *Toxoplasma gondii* in primed effector macrophages. *J. Exp. Med.* **203**, 2063–2071 (2006).
17. Andrade, R.M., Wessendarp, M., Gubbels, M.-J., Striepen, B. & Subauste, C.S. CD40 induces macrophage anti-*Toxoplasma gondii* activity by triggering autophagy-dependent fusion of pathogen-containing vacuoles and lysosomes. *J. Clin. Invest.* **116**, 2366–2377 (2006).
18. Singh, S.B., Davis, A.S., Taylor, G.A. & Deretic, V. Human IRGM induces autophagy to eliminate intracellular mycobacteria. *Science* **313**, 1438–1441 (2006).
19. Xu, Y. *et al.* Toll-like receptor 4 is a sensor for autophagy associated with innate immunity. *Immunity* **27**, 135–144 (2007).
20. Delgado, M.A., Elmaoued, R.A., Davis, A.S., Kyei, G. & Deretic, V. Toll-like receptors control autophagy. *EMBO J.* **27**, 1110–1121 (2008).
21. Sanjuan, M.A. *et al.* Toll-like receptor signalling in macrophages links the autophagy pathway to phagocytosis. *Nature* **450**, 1253–1257 (2007).
22. Mansfield, B.E., Dionne, M.S., Schneider, D.S. & Freitag, N.E. Exploration of host-pathogen interactions using *Listeria monocytogenes* and *Drosophila melanogaster*. *Cell. Microbiol.* **5**, 901–911 (2003).
23. Hamon, M., Bierne, H. & Cossart, P. *Listeria monocytogenes*: a multifaceted model. *Nat. Rev. Microbiol.* **4**, 423–434 (2006).
24. Jones, S. & Portnoy, D.A. Characterization of *Listeria monocytogenes* pathogenesis in a strain expressing perfringolysin O in place of listeriolysin O. *Infect. Immun.* **62**, 5608–5613 (1994).
25. Goto, A. Kadowaki, T. and Kitagawa, Y. *Drosophila* hemolectin gene is expressed in embryonic and larval hemocytes and its knock down causes bleeding defects. *Dev. Biol.* **264**, 582–591 (2003).
26. Scott, R.C., Schuldiner, O. & Neufeld, T.P. Role and regulation of starvation-induced autophagy in the *Drosophila* fat body. *Dev. Cell* **7**, 167–178 (2004).
27. Rusten, T.E. *et al.* Programmed autophagy in the *Drosophila* fat body is induced by ecdysome through regulation of the PI3K pathway. *Dev. Cell* **7**, 179–192 (2004).
28. Py, B.F., Lipinski, M.M. & Yuan, J. Autophagy limits *Listeria monocytogenes* intracellular growth in the early phase of primary infection. *Autophagy* **3**, 117–125 (2007).
29. Noda, T. & Ohsumi, Y. Tor, a phosphatidylinositol kinase homologue, controls autophagy in yeast. *J. Biol. Chem.* **273**, 3963–3966 (1998).
30. Scott, R.C., Juhasz, G. & Neufeld, T.P. Direct induction of autophagy by Atg1 inhibits cell growth and induces apoptotic cell death. *Curr. Biol.* **17**, 1–11 (2007).
31. Cheng, L.W. & Portnoy, D.A. *Drosophila* S2 cells: an alternative infection model for *Listeria monocytogenes*. *Cell. Microbiol.* **5**, 875–885 (2003).
32. Agaisse, H. *et al.* Genome-wide RNAi screen for host factors required for intracellular bacterial infection. *Science* **309**, 1248–1251 (2005).
33. Mizushima, N., Yamamoto, A., Matsui, M., Yoshimori, T. & Ohsumi, Y. In vivo analysis of autophagy in response to nutrient starvation using transgenic mice expressing a fluorescent autophagosome marker. *Mol. Biol. Cell* **15**, 1101–1111 (2004).
34. Kabeya, Y. *et al.* LC3, a mammalian homologue of yeast Apg8p, is localized in autophagosome membranes after processing. *EMBO J.* **19**, 5720–5728 (2000).

35. Kaneko, T. *et al.* Monomeric and polymeric gram-negative peptidoglycan but not purified LPS stimulate the *Drosophila* IMD pathway. *Immunity* **20**, 637–649 (2004).
36. Kitaura, Y. *et al.* N_{γ}-(L-α-glutamyl)-*meso*-2,,2'α-diaminopimelic acid as the minimal prerequisite structure of FK-156: its acyl derivatives with potent immunostimulating activity. *J. Med. Chem.* **25**, 335–337 (1982).
37. Sun, X., Yin, J., Starovansnik, M.A., Fairbrother, W.J. & Dixit, V.M. Identification of a novel homotypic interaction motif required for the phosphorylation of receptor-interacting protein (RIP) by RIP3. *J. Biol. Chem.* **277**, 9505–9511 (2002).
38. Meylan, E. *et al.* RIP1 is an essential mediator of Toll-like receptor 3–induced NF-κB activation. *Nat. Immunol.* **5**, 503–507 (2004).
39. Gottar, M. *et al.* The *Drosophila* immune response against Gram-negative bacteria is mediated by a peptidoglycan recognition protein. *Nature* **416**, 640–644 (2002).
40. Kotani, S., Watanabe, Y., Shimono, T., Kinoshita, F. & Narita, T. Immunoadjuvant activities of peptidoglycan subunits from the cell walls of *Staphylococcus aureus* and *Lactobacillus plantarum*. *Biken J.* **18**, 93–103 (1975).

J Periodont Res 2008; 43: 585–593

JOURNAL OF PERIODONTAL RESEARCH
doi:10.1111/j.1600-0765.2008.01096.x

Expression of functional Toll-like receptors and nucleotide-binding oligomerization domain proteins in murine cementoblasts and their upregulation during cell differentiation

E. Nemoto[1], T. Honda[1], S. Kanaya[1], H. Takada[2], H. Shimauchi[1]
Departments of [1]Periodontology and Endodontology and [2]Microbiology and Immunology, Tohoku University Graduate School of Dentistry, Sendai, Japan

Nemoto E, Honda T, Kanaya S, Takada H, Shimauchi H. Expression of functional Toll-like receptors and nucleotide-binding oligomerization domain proteins in murine cementoblasts and their upregulation during cell differentiation. J Periodont Res 2008; 43: 585–593. © 2008 The Authors. Journal compilation © 2008 Blackwell Munksgaard

Background and Objective: While the primary role of cementoblasts is to synthesize the components of cementum, we have reported that immortalized murine cementoblasts (OCCM-30) express functional Toll-like receptor (TLR)-2 and -4, and these receptors are involved in the alteration of gene expression associated with cementum formation and in the upregulation of osteoclastogenesis-associated molecules, such as receptor activator of nuclear factor-κB (NF-κB) ligand. We hypothesized that cementoblasts express a wide range of pattern recognition receptors in a manner comparable to osteoblasts, which are known to express various functional TLRs and nucleotide-binding oligomerization domain (NOD) proteins.

Material and Methods: Murine cementoblasts and pre-osteoblasts were used. The gene and protein levels of TLRs/NODs were analyzed using real-time polymerase chain reaction and flow cytometry. Interleukin-6 (IL-6) and activated NF-κB were measured using enzyme-linked immunosorbent assay.

Results: The expressions of TLR-1, -2, -4, -6 and -9, CD14, NOD-1 and -2 were detected in cementoblasts and were upregulated upon differentiation induced by ascorbic acid. Similar patterns were observed in the mouse MC3T3-E1 osteoblast cell line. Synthetic ligands, Pam3CSK4 (TLR-1/2 agonist), Pam2CGDPKHPKSF (TLR-2/6 agonist), lipid A (TLR4 agonist), CpG DNA (TLR-9 agonist), FK565 (NOD1 agonist) and muramyldipeptide (NOD2 agonist), effectively induced NF-κB activation in cementoblasts and/or ascorbic acid-treated cementoblasts. Furthermore, these ligands induced IL-6 production in a NF-κB-dependent manner in cementoblasts and/or ascorbic acid-treated cementoblasts.

Eiji Nemoto, DDS, PhD, Department of Periodontology and Endodontology, Tohoku University Graduate School of Dentistry, 4-1 Seiryo-machi Aoba, Sendai 980-8575, Japan
Tel: +81 22 717 8334
Fax: +81 22 717 8339
e-mail: e-nemoto@umin.ac.jp

Key words: cementoblast; Toll-like receptor; nucleotide-binding oligomerization domain protein; differentiation

Accepted for publication March 6, 2008

Conclusion: These results indicate that cementoblasts possess functional TLR and NOD signaling systems and have a similar capacity to osteoblasts in responding to a wide variety of pathogens.

The innate immune system is initiated by the recognition of conserved motifs in pathogens termed 'pathogen-associated molecular patterns' (PAMPs). Members of the Toll-like receptor (TLR) family and CD14 are essential components in this process. To date, at least 12 members of the TLR family have been identified in mammalian systems as pattern recognition receptors (PRRs; 1). Toll-like receptor-4 recognizes lipopolysaccharide (LPS) from gram-negative bacteria (2). Toll-like receptor-2 recognizes a diverse set of pathogen-associated motifs including peptidoglycan, lipoproteins/lipopeptides and lipoteichoic acid from various microorganisms (1). It has been demonstrated that this broader ligand specificity (3) is attributed to the unique ability of TLR-2 to heterodimerize with TLR-1 and TLR-6 for the recognition of triacylated and diacylated lipoprotein, respectively (4,5). Toll-like receptor-9 recognizes bacterial DNA in a manner dependent on unmethylated cytosin-phosphorothioate-guanine (CpG) dinucleotides in particular base contexts, which are termed CpG motifs (6). CD14 not only facilitates the binding of LPS to the TLR-4–myeloid differentiation protein (MD)-2 complex (7), but has also been reported to bind directly to triacylated lipopeptides and facilitate recognition of the lipopeptides by the TLR-2–TLR-1 complex (8). Recently, a family of nucleotide-binding oligomerization domain (NOD) proteins has been identified as intracellular PRRs. NOD1 interacts with motifs found in peptidoglycans carrying *meso*-diaminopimelic acid (*meso*-DAP), which is found in most gram-negative and some gram-positive bacteria (9,10). In contrast, NOD2 has been implicated as a general sensor of bacterial peptidoglycans because it recognizes a minimal motif present in almost all peptidoglycans, muramyldipeptides MurNAc-L-Ala-D-isoGln (MDP) or MurNAc-L-Ala-D-Glu (11,12).

Cementum is a thin mineralized tissue covering the tooth root surface that shares many properties with bone (13) and most notably a remarkable similarity in biochemical composition (14). However, cementum differs from bone in its histology by lacking innervation and vascularization. In addition, cementum has no bone marrow and limited remodeling potential when compared with bone, where a system consisting of osteoblasts, osteocytes, bone-lining cells and osteoclasts is required (15).

While the primary role of cementoblasts and osteoblasts is to synthesize the components of cementum and bone matrix, respectively, it has been reported that osteoblasts exhibit functional expression of TLR-2, TLR-4 (16,17), TLR-5 (18), TLR-9 (6), NOD1 (19) and NOD2 (19,20) and initiate the release of inflammatory cytokines and osteoclastogenesis by activating these receptors. For example, *Escherichia coli* LPS interacts with TLR-4 on the surface of osteoblasts and upregulates the expression of receptor activator of nuclear factor-κB (NF-κB) ligand (RANKL) and downregulates the expression of osteoprotegerin (OPG), which acts as a decoy receptor for RANKL (17,21). The CpG oligodeoxynucleotides interact with osteoblastic TLR-9 and increase the expression of molecules regulating osteoclastogenesis (6). Furthermore, NOD2-mediated signals are involved in MDP-induced RANKL expression in osteoblasts (20). Recently, we reported that murine cementoblasts express functional TLR-2 and TLR-4 (22,23), and they were found to be involved in the alteration of gene expression associated with cementum formation (22) and the upregulation of osteoclastogenesis-associated molecules such as RANKL (23). These findings suggest that cementoblasts participate in the innate immune system in a way comparable to osteoblasts by expressing not only TLR-2 and TLR-4 but also other functional PRRs.

In the present study, we demonstrate that murine cementoblasts express TLR-1, -2, -4, -6 and -9, CD14, NOD1 and NOD2 and their adaptor molecules at the gene and/or protein levels and that the expression levels of PRRs are upregulated in the course of cell differentiation. Furthermore, we show that these PRRs are functional receptors using synthetic chemical ligands specific for the respective TLRs and NODs.

Material and methods

Reagents

Biotin-conjugated monoclonal antibodies (mAbs) for mouse TLR-1 (eBioTR23), mouse TLR-2 (T2.5, mouse IgG_1), mouse TLR-4/MD-2 (MTS510, Rat IgG_{2a}), fluorescein isothiocyanate (FITC)-conjugated mAbs for mouse TLR-9 (M9.D6), mouse CD14 (Sa2-8), rat IgG_{2a} isotype control antibody and phycoerythrin (PE)-conjugated streptavidin were purchased from eBioscience (San Diego, CA, USA). Anti-mouse TLR-6 (rabbit polyclonal) was from IMGENEX (San Diego, CA, USA). Anti-rabbit IgG (H + L; goat polyclonal, fluor 488) was from AnaSpec, Inc. (San Jose, CA, USA). Pyrrolidine dithiocarbamat (PDTC, a NF-κB inhibitor) was purchased from Calbiochem-Novabiochem Co. (La Jolla, CA, USA). All tissue culture reagents were purchased from Gibco BRL (Rockville, MD, USA).

Stimulants

Pam_3CSK_4 (TLR-1/2 agonist), a synthetic tripalmitoylated lipopeptide that mimics the acylated aminoterminus of bacterial lipoproteins, and Pam_2CGDPKHPKSF (TLR-2/6 agonist), a synthetic lipoprotein representing the N-terminal part of the 44 kDa lipoprotein LP44 of *Mycoplasma salivarium*, were purchased from InvivoGen (San Diego, CA, USA). Synthetic muramyldipeptide [MurNAc-L-Ala-D-isoGln (MDP); NOD2 agonist] and *E. coli*-type lipid A (LA-

15-PP; TLR-4 agonist) were purchased from Protein Research Foundation Peptide Institute (Osaka, Japan). FK565 (heptanoyl-γ-D-Glu-*meso*-DAP-D-Ala; NOD1 agonist) was supplied by Astellas Pharmaceutical Co. (Tokyo, Japan). Conventional CpG DNA (TLR-9 agonist), CpG ODN 1826 [TCCATGACGTTCCTGACGTT (CpG motif is underlined)], was purchased from Sigma-Aldrich Japan K.K. (Tokyo, Japan).

Cells

An immortalized murine cementoblast cell line (OCCM-30), established by the isolation of tooth root-surface cells from transgenic mice containing an SV40 large T-antigen under the control of the osteocalcin (OCN) promoter (24), was kindly provided by Dr Martha J. Somerman, University of Washington, WA, USA. The OCCM-30 cells were maintained in Dulbecco's modified Eagle's medium (DMEM; Gibco BRL, Rockville, MD, USA) plus 10% fetal bovine serum (FBS; Gibco BRL) and antibiotics. A murine pre-osteoblastic cell line, MC3T3-E1, was purchased from ATCC (Manassas, VA, USA) and maintained in α-minimal essential medium (α-MEM; Gibco) containing 10% FBS and antibiotics. A murine macrophage cell line, J774-1, was obtained from the Cell Resource Center for Biomedical Research, Tohoku University (Sendai, Japan) and maintained in RPMI 1640 (Nissui pharmaceutical Co., Tokyo, Japan) containing 10% FBS and antibiotics. The experimental procedures were approved by the Ethical Review Board of Tohoku University Graduate School of Dentistry (Sendai, Japan).

Cell differentiation and treatment

To induce cell differentiation, confluent OCCM-30 or MC3T3-E1 cells were cultured in DMEM and α-MEM, respectively, containing 5% FBS in the presence of 50 μg/mL ascorbic acid (Sigma, St Louis, MO, USA) and the media were changed every 3 days. After reaching confluency, the cells were treated with the indicated synthetic stimulant in medium containing 5% FBS. In some experiments, cell stimulation was performed in the presence of 1 μM cytochalasin D (Sigma), where all the samples were adjusted to contain 0.1% (v/v) DMSO in the media.

Fluorescence activated cell sorting (FACS) analysis

Confluent cells were collected using Cell Dissociation Solution® (Sigma), washed with phosphate-buffered saline three times, and used for staining. For cell surface staining, a total of 10^5 cells were stained with each mAb or isotype-matched control IgG at 4°C for 20 min. Following washing, PE-conjugated streptavidin was added at 4°C for 20 min. Intracellular staining was performed with IC Fixation/Permeabilization buffer® (eBioscience) according to the manufacturer's instructions. Fixed and permeabilized cells were stained with FITC-conjugated mAbs or isotype-matched IgG for 20 min. Staining was analyzed on a FACSCalibur cytometer® (Becton Dickinson, Mountain View, CA, USA). The arithmetic mean was used in the computation of the mean fluorescence intensity (MFI).

Quantitative real-time reverse transcriptase-polymerase chain reaction (RT-PCR)

Total cellular RNA was extracted using TRIzol® reagent (Gibco) according to the manufacturer's instructions, and was DNase-treated (DNA-free™; Ambion Inc., Austin, TX, USA). The transcription of total RNA into cDNA was carried out with the use of a Transcriptor First Strand cDNA Synthesis Kit® (Roche Diagnostic Co., Indianapolis, IN, USA) according to the manufacturer's instructions. The primer sequences for each gene, TLR-1, TLR-2, TLR-4, TLR-6, TLR-9, CD14, NOD1, NOD2, alkaline phosphatase (ALP), OCN and glyceraldehyde 3-phosphate dehydrogenase (GAPDH), are shown in Table 1. The amplification profile was 40 cycles at 95/60; 55/30; 72/30 [temperature (°C)/time (s)]. The PCR was performed in an iCycler (Bio-Rad Laboratories, Hercules, CA, USA) with iQ SYBR Green Supermix (Bio-Rad) with optimized levels of 3 mM $MgCl_2$ and 0.5 μM of each primer. After amplification, one cycle of linear temperature gradient from 55 to 95°C at a transition rate of 0.5°C/30 s was performed to assess the specificity of the PCR products. For each run, water was used as the negative control. Reaction products were quantified with GAPDH as the reference gene. Since J774-1 and OCCM-30 are regarded as representative cells expressing functional TLRs/NODs and ALP/OCN, respectively, cDNA samples from these cells were used as calibrators for TLRs/NODs and ALP/OCN expression, respectively. Therefore, the value on the *Y* axis of the figures 2 and 3 indicates the fold-increase vs. the gene expression level in J774-1 or OCCM-30 cells. For conventional PCR, the

Table 1. Primer sequence used for polymerase chain reaction amplifications

Gene	Primer sequences forward/reverse
OCN	TGAACAGACTCCGGCG/GATACCGTAGATGCGTTTG
ALP	GGGGACATGCAGTATGAGTT/GGCCTGGTAGTTGTTGTGAG
TLR-1	TCTCTTCGGCACGTTAGC/CGTAAGAAATAAGAGCAGCCC
TLR-2	CGAGTGGTGCAAGTACG/GGTAGGTCTTGGTGTTCATTATC
TLR-4	GCAGCAGGTGGAATTGTATC/TGTTCTTCCTCTGCTGTTTG
TLR-6	CCGGTGGAGTACCTCAAT/TCAGCAAACACCGAGTATAGC
TLR-9	CTGCCGCTGACTAATCTG/CTGAAATTGTGGCCTATACCC
CD14	TCTCAGTTACAACAGGCTGGATA/CACTGCTTGGGATGATGG
NOD-1	GGACAACTTGCTGGAGAAT/CTGCAGCACGTAGAGGAA
NOD-2	CTTCATTTGGCTCATCCGTAG/CTGGAGATGTTGCAGTACAAAG
MyD88	TGATGCGGAGCCAGATT/GAGGAGGCATGTGTGTACT
TIRAP	GCTGAAGATGGGAACCAC/CTGCTGACCTTCCCGAT
IRAK4	CCAAATCTGACATCTACAGCTT/CATCCGTGTAATCTTCAATCG
Rip2 kinase	GGAGGAACAATCATCTATATGCC/ATGATCTGCAAAGGATTGGT
GAPDH	ACCACAGTCCATGCCATCAC/TCCACCACCCTGTTGCTGTA

amplification profile was 30 cycles using the same cycle programme (temperature/time). Amplified samples were visualized on 2.0% agarose gels stained with ethidium bromide and photographed under UV light.

Preparation of whole-cell extracts

Whole-cell extracts were prepared from confluent cells using a Nuclear Extract Kit™ (Active Motif, Carlsbad, CA, USA). Confluent cells cultured in six-well plates were harvested with a cell scraper and lysed in 75 μL of Complete lysis buffer. Cell suspensions were incubated on ice for 10 min on a rocking platform followed by centrifugation at 14,000 *g* for 20 min, and then the supernatants were collected and stored at −80°C until use. The concentration of protein in the cell lysates was measured using a *DC* Protein Assay® (Bio-Rad).

Enzyme-linked immunosorbent assay (ELISA)

The supernatants from cell cultures were harvested by centrifugation. The amount of IL-6 in the supernatant was measured using a mouse ELISA kit (BioSource International Inc., Camarillo, CA, USA). The assay was performed according to the manufacturer's instructions. Results were normalized to protein level using a standard curve. Each sample was assayed in triplicate.

Nuclear factor-κB ELISA

Activated NF-κB was measured with a TransAM™ NF-κB p65 transcription factor assay kit according to the manufacturer's instructions (Active Motif, Carlsbad, CA, USA). Briefly, whole-cell extracts (10 μg of protein per well) were added to 96-well plates coated with oligonucleotide containing the NF-κB consensus site (5′-GGGACTTTCC-3′) and incubated for 1 h at room temperature. After washing, the wells were incubated with NF-κB antibody for 1 h at room temperature followed by incubation with horseradish peroxidase-conjugated anti-rabbit IgG for 1 h at room temperature. Colorimetric reactions were developed and measured at 450 nm. For a positive control, the provided Jurkat cell nuclear extract (2.5 μg of protein per well) was used. Results were expressed as means of the value of optical density at 450 nm of triplicate measurements.

Statistical analysis

All experiments in this study were performed three times to test the reproducibility of the results, and representative findings are shown. Experimental values are given as means ± SD. The significance of differences between control and treatments was evaluated by one-way ANOVA. Values of $p < 0.05$ were considered significant.

Results

Expression of TLRs and CD14 at the protein level in cementoblasts and osteoblasts

We examined the possible expression of PRRs in cementoblasts and osteoblasts by flow cytometry. Confluent cultured (designated as day 0 cells) cementoblasts as well as osteoblasts expressed TLR-2, TLR-9 and CD14. The levels of TLR-2 expression in these cells were substantially comparable with that in the murine macrophage cell line, J774-1, which was used as a positive control, but the levels of TLR-9 and CD14 were much lower than that in J774-1. When the cells were cultured with ascorbic acid for 5 days (designated as day 5 cells), the expression levels of TLR-2 and TLR-9 in cementoblasts and the expression of TLR-9 and CD14 in osteoblasts were enhanced. Unlike J774-1 cells, which expressed significant levels of TLR-1, TLR-4 and TLR-6, both types of day 0 cells showed limited or slight expression of TLR-1, TLR-4 and TLR-6. Levels of TLR-1 and TLR4 in both cell types and TLR-6 in osteoblasts increased upon differentiation (Fig. 1).

Expression of TLRs, CD14 and NODs at the gene level in cementoblasts and osteoblasts

We next examined the gene expression of PRRs, including NOD1 and NOD2, in the course of cell differentiation. Cementoblasts were induced to differentiate by culturing in the presence of ascorbic acid over a 5 day period with ALP and OCN used as reference index genes (Fig. 2A). During cell differentiation, all PRRs were upregulated, with

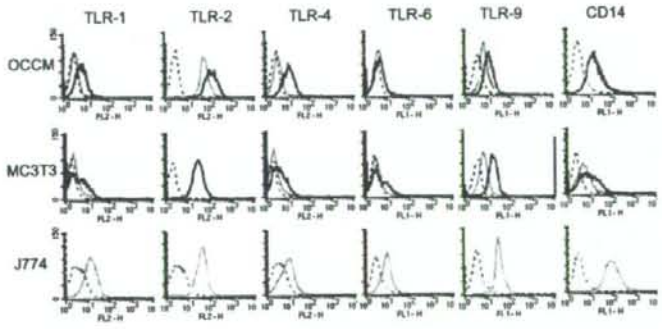

Fig. 1. Expression of TLR-1, -2, -4, -6 and -9 and CD14 at the protein level in cementoblasts, osteoblasts and macrophage cell lines. The OCCM-30 (cementoblasts) and MC3T3-E1 cells (osteoblasts) were cultured in DMEM and α-MEM, respectively, containing 5% FBS until confluent (day 0 cells; red lines), and then differentiation was induced by the addition of ascorbic acid (50 μg/mL) for 5 days (day 5 cells; blue line). The J774-1 cells (macrophage cell line) were cultured in RPMI 1640 containing 5% FBS until subconfluent (red line). After being harvested by cell dissociation solution (non-enzymatic), cells were stained with each TLR and CD14 antibody and analyzed by FACS. Representative data of three separate experiments are shown. Dotted line represents the isotype control staining (FL1:FITC, FL2:PE).

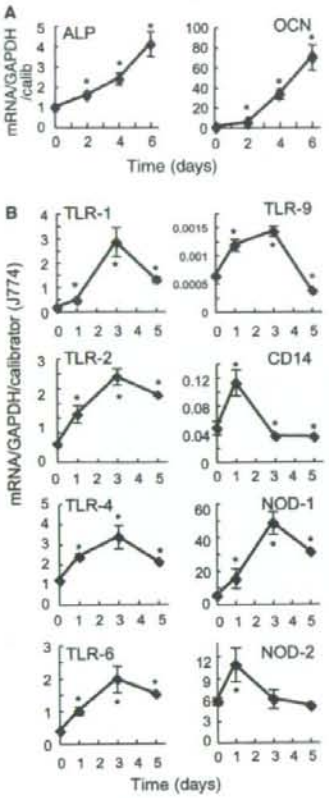

Fig. 2. Expression of TLR-1, -2, -4, -6 and -9, CD14, NOD1 and NOD2 at the gene level in cementoblasts. Confluent OCCM-30 cells were cultured in DMEM containing 5% FBS in the presence of ascorbic acid (50 μg/mL) for the indicated time periods. Total cellular RNA was extracted, and the mRNA expression levels were analyzed by real-time quantitative RT-PCR. Representative data of three separate experiments are shown as means ± SD of triplicate assays. Statistical significance is shown (*$p < 0.05$ vs. day 0 control).

a peak at days 1–3 (Fig. 2B). The expressions of TLR-9 and CD14 were lower by approximately three and one order(s) of magnitude, respectively, compared with those of J774-1, which is consistent with the protein expression levels shown in Fig. 1. The gene expression level of TLR-6, which was limited at the protein level in cementoblasts (days 0 and 5) shown in Fig. 1, was detected at day 0 and was significantly induced upon differentiation. The expression of NOD1 and NOD2 increased approximately 50- and twofold, respectively, upon differentiation (Fig. 2B). Osteoblasts were induced to differentiate by the addition of ascorbic acid over a 6 day period using reference index genes ALP and OCN shown in Fig. 3A. In Fig. 3B, osteoblasts are shown to exhibit very similar trends to those of cementoblasts except that the peak periods varied.

Expression of key downstream effector molecules for TLR and NOD signaling in cementoblasts and osteoblasts

In order to begin determining whether cementoblasts express functional TLRs and NODs, we examined whether cementoblasts express downstream effector molecules (1) by RT-PCR. Myeloid differentiation factor 88 (MyD88) is a common adaptor molecule for TLR signaling. Interleukin-1 receptor-associated kinase (IRAK) 4 and Toll/interleukin-1 receptor (TIR) domain-containing adaptor protein (TIRAP) are essential for the MyD88-dependent signaling pathway. Receptor-interacting protein (Rip) 2 kinase is a critical effector molecule in both NOD1- and NOD2-mediated cellular activation (25). Confluent cementoblasts and osteoblasts constitutively expressed the mRNAs for these signaling molecules (Fig. 4).

Activation of NF-κB in cementoblasts upon stimulation with synthetic chemical TLR and NOD ligands

Since most of the TLR and NOD signaling pathways mainly lead to the activation of NF-κB, we examined whether TLRs and NODs expressed by cementoblasts were functional in terms of NF-κB activation upon stimulation with their respective ligands. Pam_3CSK_4 (TLR-1/2 agonist), but not $Pam_2CGDPKHPKSF$ (TLR-2/6 agonist) or lipid A (TLR-4 agonist), significantly activated NF-κB in confluent cementoblasts (day 0 cells; Fig. 5A). Activation of NF-κB was significantly induced upon stimulation with Pam_3CSK_4, $Pam_2CGDPKHPKSF$ and lipid A in day 2 cells (Fig. 5A). In contrast, NF-κB activation was marginal after treatment with CpG DNA (TLR-9 agonist), FK565 (NOD1 agonist) or muramyldipeptide (NOD2 agonist; data not shown). Since TLR-9 and NODs are intracellular receptors, cells were pretreated with cytochalasin D (1 μM) to facilitate stimulation by

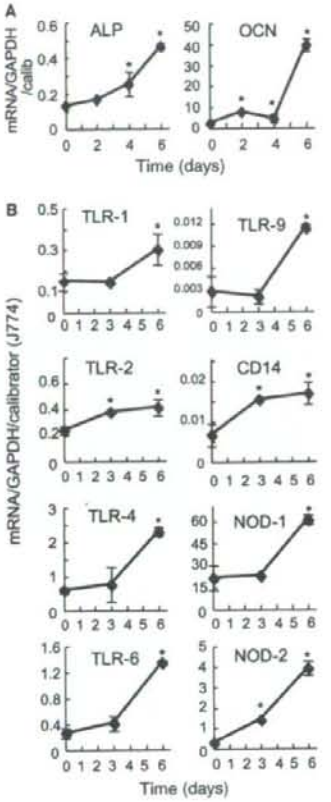

Fig. 3. Expression of TLR-1, -2, -4, -6 and -9, CD14, NOD1 and NOD2 at the gene level in osteoblasts. Confluent MC3T3 cells were cultured in α-MEM containing 5% FBS in the presence of ascorbic acid (50 μg/mL) for the indicated time periods. Total cellular RNA was extracted and the mRNA expression levels were analyzed by real-time quantitative RT-PCR. Representative data of three separate experiments are shown as means ± SD of triplicate assays. Statistical significance is shown (*$p < 0.05$ vs. day 0 control).

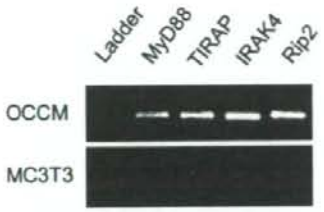

Fig. 4. Expression of key downstream effector molecules for TLR and NOD signaling in cementoblasts and osteoblasts. Total cellular RNA was extracted from confluent OCCM-30 and MC3T3 cells, and the mRNA expression levels of MyD88, TIRAP, IRAK4 and Rip2 kinase were analyzed by RT-PCR. Representative data of three separate experiments are shown.

TLR-9 and NOD ligands (26). It has been well established that cytochalasin D inhibits actin polymerization and allows components to internalize into the cells (27). Activation of NF-κB was detected upon stimulation with FK565, muramyldipeptide and CpG DNA in both day 0 and day 2 cells (Fig. 5B).

Effect of an NF-κB inhibitor on IL-6 production induced by synthetic TLR and NOD ligands

Next, we examined whether TLRs and NODs on cementoblasts are functional in terms of IL-6 production using ELISA. A major function of IL-6, as related to bone, is the induction of osteoclast activity, although it is recognized that IL-6 is a pleiotropic cytokine that has both pro- and anti-inflammatory actions (28). Agonists for TLR-1/2, TLR-2/6 and TLR-4 significantly induced IL-6 production in day 0 cells, and much higher production was observed in day 2 cells (Fig. 6A). Since TLR-9 and NODs are intracellular receptors, day 0 cells were stimulated with these agonists in the presence of cytochalasin D. Significant induction, especially by the NOD2 agonist, was observed for all stimulants (Fig. 6B). When day 2 cells were stimulated in the same way as day 0 cells, much higher production of IL-6 was observed (Fig. 6B). These findings were consistent with the results shown in Figs 1–3, where differentiated cells showed higher expression of TLRs and NODs compared with day 0 cells. All of the inductions in day 0 and day 2 cells were completely inhibited to background levels or lower by pretreatment with 100 μM of PDTC, a NF-κB inhibitor (Fig. 6A,B). These results indicate that cementoblasts express functional TLRs and NODs, the signaling from which is capable of activating NF-κB and leads to IL-6 production.

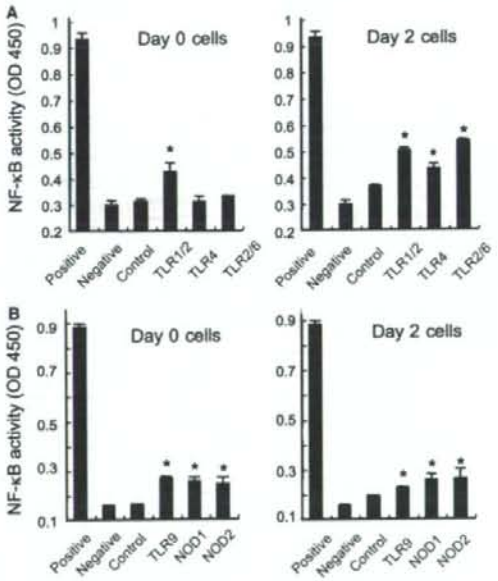

Fig. 5. Activation of NF-κB in cementoblasts triggered by TLR and NOD ligands. Confluent OCCM-30 cells (day 0 cells) were cultured in DMEM containing 5% FBS in the presence of ascorbic acid (50 μg/mL) for 2 days (day 2 cells). (A) Both day 0 and day 2 cells were stimulated with 1 μg/mL Pam_3CSK_4 (TLR-1/2 agonist), 1 μg/mL $Pam_2CGDPKHPKSF$ (TLR-2/6 agonist) or 100 ng/mL lipid A (TLR-4 agonist) for 3 h in DMEM with 5% FBS. (B) Cells were stimulated with 5 μM CpG DNA (TLR-9 agonist), 100 μg/mL FK565 (NOD1 agonist), or 100 μg/mL muramyldipeptide (NOD2 agonist) for 3 h in DMEM with 5% FBS in the presence of cytochalasin D (1 μM) in the same medium to facilitate stimulation by intracellular receptor ligands. All the samples, including the control sample, were adjusted to contain 0.1% (v/v) DMSO in the media during cell culture. After stimulation, whole cell extracts were prepared and a NF-κB ELISA assay was performed. The positive control was provided by a nuclear extract of Jurkat cells. A sample with no cell extract was used as a negative control. Representative data of three separate experiments are shown as means ± SD of triplicate assays. Statistical significance is shown (*$p < 0.05$ vs. day 0 cell control).

Discussion

We have demonstrated that murine cementoblasts as well as osteoblasts express TLR-1, -2, -4, -6 and -9, CD14, NOD1 and NOD2, as well as their adaptor molecules, MyD88, TIRAP, IRAK4 and Rip2 kinase. Furthermore, we showed that the respective ligands induce IL-6 production via NF-κB activation, where CD14 may serve to facilitate ligand recognition by TLR-1/2 as well as TLR-4. These findings suggest that cementoblasts have a similar capacity to osteoblasts to respond to a wide variety of pathogens. However, it has been reported that there are not only similarities but also differences in terms of the reactivity to these ligands. Toll-like receptor-4 signaling triggered by *E. coli* LPS induces production of cytokines, including IL-6, and upregulates RANKL expression in both cell types (17,20,23,29). Toll-like receptor-2 signaling also

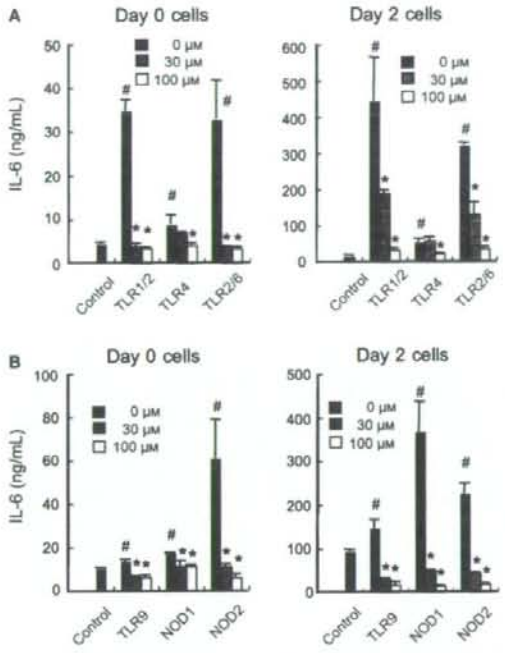

Fig. 6. Interleukin-6 production in cementoblasts triggered by TLR and NOD ligands. Confluent OCCM-30 cells (day 0 cells) were cultured in DMEM containing 5% FBS in the presence of ascorbic acid (50 μg/mL) for 2 days (day 2 cells). Both day 0 and day 2 cells were pretreated with/without the indicated concentrations of PDTC, a NF κB inhibitor, for 1 h. (A) Cells were stimulated with 1 μg/mL Pam3CSK4 (TLR-1/2 agonist), 1 μg/mL Pam2CGDPKHPKSF (TLR-2/6 agonist) or 100 ng/mL lipid A (TLR-4 agonist) in DMEM containing 5% FBS for 12 h. (B) Cells were stimulated with 5 μM CpG DNA (TLR-9 agonist), 100 μg/mL FK565 (NOD1 agonist) or 100 μg/mL muramyldipeptide (NOD2 agonist) in the presence of cytochalasin D (1 μM) in DMEM containing 5% FBS for 24 h. All the samples, including the control sample, were adjusted to contain 0.1% (v/v) DMSO in the media during cell culture. The amount of IL-6 in the supernatants was analyzed by ELISA. Representative data of three separate experiments are shown as means ± SD of triplicate assays. $*p < 0.05$ vs. respective control; $p < 0.05$ vs. control culture.

upregulates RANKL in both cell types (23,30). In contrast, OPG, which is downregulated by *E. coli* LPS in osteoblasts (17,20), is constitutively expressed and not altered in cementoblasts under the same stimulation conditions (23), suggesting that cementoblasts, unlike osteoblasts, may have inhibitory properties for osteoclastogenesis generated by the innate immunity response. This notion is consistent with the clinical observation that root resorption is rarely linked to periodontal disease, even at a stage of severe disease with marked resorption of alveolar bone. In periapical inflammatory lesions, bone resorption can usually be observed rather than external periapical root resorption, although periforaminal resorption has been associated with it (31).

We demonstrated that the expressions of TLRs and NODs were upregulated upon differentiation in both cementoblasts and osteoblasts in a similar manner; however, gene expression levels over 5 days of differentiation were quite different. The OCCM-30 cell line was established based on *in situ* hybridization data, i.e. only cementoblasts expressed strong bone sialoprotein (BSP) and OCN gene signals, while PDL cells did not (24). The OCCM-30 cell line is considered as a mature cell line because it expresses high levels of BSP and OCN transcripts. In contrast, precursor cell lines, such as MC3T3-E1 cells, require additional factors to initiate the expression of BSP and OCN. The OCCM-30 (24) and MC3T3-E1 cell lines (32) require several days and 2 weeks, respectively, before mineralized nodules are formed in the presence of ascorbic acid *in vitro*. Therefore, the different gene expression levels are probably due to the different maturation stage of the cells.

It has been reported that the expression levels of TLR-2 (16,17), NOD1 and NOD2 (19,20) mRNAs in mouse osteoblasts are increased by *E. coli* LPS and exposure to bacteria. Since the promoter regions of these genes possess NF-κB binding site(s) (33,34), activation of NF-κB has been implicated in the induction of mouse TLR-2 and NOD2 expression. In this study, we showed that the expression of TLRs and NODs was upregulated upon differentiation induced by ascorbic acid. However, NF-κB does not seem to be involved in this regulation, since ascorbic acid was reported to inhibit NF-κB activation (35).

Another question that arises is, why do cementoblasts and osteoblasts, which do not even reside in the first line in bacterial challenge, need to amplify PRR expression in the course of cell differentiation? Recent evidence suggests that TLR-2 and TLR-4 are involved in the recognition not only of microbes but also of endogenous ligands, including heat shock proteins (36,37) and extracellular matrix components, such as fibronection (38), soluble hyaluronic acid (39), heparan sulfate (40) and biglycan (41). Therefore, upregulation of TLRs during cell differentiation, while speculative at this point, might be involved in the recognition of endogenous ligands.

In conclusion, we report for the first time that cementoblasts functionally express a wide range of PRRs, and the upregulation of these receptors accompanies cell differentiation. The alteration of cell function mediated by TLR/NOD signaling needs to be explored further in order for us to understand the role of cementoblasts in

inflammation/regeneration in periodontal tissue.

Acknowledgements

We gratefully acknowledge Dr Martha J. Somerman (University of Washington, Seattle, WA, USA) for helpful discussions. This work was supported by a Grant-in-Aid for Scientific Research (19592380) and Grant-in-Aid for Exploratory Research (19659546) from the Japan Society for the Promotion of Sciences. We thank D. Mrozek (Medical English Service, Kyoto, Japan) for reviewing this manuscript.

References

1. Takeda K, Kaisho T, Akira S. Toll-like receptors. *Annu Rev Immunol* 2003; **21**:335–376.
2. Hoshino K, Takeuchi O, Kawai T *et al.* Toll-like receptor 4 (TLR4)-deficient mice are hyporesponsive to lipopolysaccharide: evidence for TLR4 as the *Lps* gene product. *J Immunol* 1999;**162**:3749–3752.
3. Ozinsky A, Underhill DM, Fontenot JD *et al.* The repertoire for pattern recognition of pathogens by the innate immune system is defined by cooperation between toll-like receptors. *Proc Natl Acad Sci U S A* 2000;**97**:13766–13771.
4. Takeuchi O, Kawai T, Mühlradt PF *et al.* Discrimination of bacterial lipoproteins by Toll-like receptor 6. *Int Immunol* 2001;**13**:933–940.
5. Takeuchi O, Sato S, Horiuchi T *et al.* Role of Toll-like receptor 1 in mediating immune response to microbial lipoproteins. *J Immunol* 2002;**169**:10–14.
6. Zou W, Amcheslavsky A, Bar-Shavit Z. CpG oligodeoxynucleotides modulate the osteoclastogenic activity of osteoblasts via Toll-like receptor 9. *J Biol Chem* 2003; **278**:16732–16740.
7. Akashi S, Saitoh S, Wakabayashi Y *et al.* Lipopolysaccharide interaction with cell surface Toll-like receptor 4-MD-2: higher affinity than that with MD-2 or CD14. *J Exp Med* 2003;**198**:1035–1042.
8. Nakata T, Yasuda M, Fujita M *et al.* CD14 directly binds to triacylated lipopeptides and facilitates recognition of the lipopeptides by the receptor complex of Toll-like receptors 2 and 1 without binding to the complex. *Cell Microbiol* 2006;**8**:1899–1909.
9. Girardin SE, Boneca IG, Carneiro LA *et al.* Nod1 detects a unique muropeptide from gram-negative bacterial peptidoglycan. *Science* 2003;**300**:1584–1587.
10. Chamaillard M, Hashimoto M, Horie Y *et al.* An essential role for NOD1 in host recognition of bacterial peptidoglycan containing diaminopimelic acid. *Nat Immunol* 2003;**4**:702–707.
11. Girardin SE, Boneca IG, Viala J *et al.* Nod2 is a general sensor of peptidoglycan through muramyl dipeptide (MDP) detection. *J Biol Chem* 2003;**278**:8869–8872.
12. Inohara N, Ogura Y, Fontalba A *et al.* Host recognition of bacterial muramyl dipeptide mediated through NOD2. Implications for Crohn's disease. *J Biol Chem* 2003;**278**:5509–5512.
13. Tenorio D, Cruchley A, Hughes FJ. Immunocytochemical investigation of the rat cementoblast phenotype. *J Periodont Res* 1993;**28**:411–419.
14. Birkedal-Hansen H, Butler WT, Taylor RE. Proteins of the periodontium. Characterization of the insoluble collagens of bovine dental cementum. *Calcif Tissue Res* 1977;**23**:39–44.
15. Bosshardt DD. Are cementoblasts a subpopulation of osteoblasts or a unique phenotype? *J Dent Res* 2005;**84**: 390–406.
16. Gasper NA, Petty CC, Schrum LW, Marriott I, Bost KL. Bacterium-induced CXCL10 secretion by osteoblasts can be mediated in part through toll-like receptor 4. *Infect Immun* 2002;**70**:4075–4082.
17. Kikuchi T, Matsuguchi T, Tsuboi N *et al.* Gene expression of osteoclast differentiation factor is induced by lipopolysaccharide in mouse osteoblasts via Toll-like receptors. *J Immunol* 2001;**166**: 3574–3579.
18. Madrazo DR, Tranguch SL, Marriott I. Signaling via Toll-like receptor 5 can initiate inflammatory mediator production by murine osteoblasts. *Infect Immun* 2003;**7**:5418–5421.
19. Marriott I, Rati DM, McCall SH, Tranguch SL. Induction of Nod1 and Nod2 intracellular pattern recognition receptors in murine osteoblasts following bacterial challenge. *Infect Immun* 2005; **73**:2967–2973.
20. Yang S, Takahashi N, Yamashita T *et al.* Muramyl dipeptide enhances osteoclast formation induced by lipopolysaccharide, IL-1α, and TNFα through nucleotide-binding oligomerization domain-2-mediated signaling in osteoblasts. *J Immunol* 2005;**175**:1956–1964.
21. Suda K, Udagawa N, Sato N *et al.* Suppression of osteoprotegerin expression by prostaglandin E_2 is crucially involved in lipopolysaccharide-induced osteoclast formation. *J Immunol* 2004;**172**:2504–2510.
22. Nociti FH Jr, Foster BL, Barros SP, Darveau RP, Somerman MJ. Cementoblast gene expression is regulated by *Porphyromonas gingivalis* lipopolysaccharide partially via toll-like receptor-4/MD-2. *J Dent Res* 2004;**83**:602–607.
23. Nemoto E, Darveau RP, Foster BL, Nogueira-Filho GR, Somerman MJ. Regulation of cementoblast function by *P. gingivalis* lipopolysaccharide via TLR2. *J Dent Res* 2006;**85**:733–738.
24. D'Errico JA, Berry JE, Ouyang H, Strayhorn CL, Windle JJ, Somerman MJ. Employing a transgenic animal model to obtain cementoblasts *in vitro*. *J Periodontol* 2000;**71**:63–72.
25. Ogura Y, Inohara N, Benito A, Chen FF, Yamaoka S, Nunez G. Nod2, a Nod1/Apaf-1 family member that is restricted to monocytes and activates NF-κB. *J Biol Chem* 2001;**276**:4812–4818.
26. Uehara A, Fujimoto Y, Kawasaki A, Kusumoto S, Fukase K, Takada H. Mesodiaminopimelic acid and meso-lanthionine, amino acids specific to bacterial peptidoglycans, activate human epithelial cells through NOD1. *J Immunol* 2006;**177**:1796–1804.
27. Gruenheid S, Finlay BB. Microbial pathogenesis and cytoskeletal function. *Nature* 2003;**422**:775–781.
28. Papanicolaou DA, Wilder RL, Manolagas SC, Chrousos GP. The pathophysiologic roles of interleukin-6 in human disease. *Ann Intern Med* 1998;**128**:127–137.
29. Ishimi Y, Miyaura C, Jin CH *et al.* IL-6 is produced by osteoblasts and induces bone resorption. *J Immunol* 1990;**145**:3297–3303.
30. Sato N, Takahashi N, Suda K *et al.* MyD88 but not TRIF is essential for osteoclastogenesis induced by lipopolysaccharide, diacyl lipopeptide, and IL-1α. *J Exp Med* 2004;**200**:601–611.
31. Vier FV, Figueiredo JAP. Prevalence of different periapical lesions associated with human teeth and their correlation with the presence and extension of apical external root resorption. *Int Endod J* 2002;**35**: 710–719.
32. Wang D, Christensen K, Chawla K, Xiao G, Krebsbach PH, Franceschi RT. Isolation and characterization of MC3T3-E1 preosteoblast subclones with distinct in vitro and in vivo differentiation/mineralization potential. *J Bone Miner Res* 1999;**14**:893–903.
33. Musikacharoen T, Matsuguchi T, Kikuchi T, Yoshikai Y. NF-κB and STAT5 play important roles in the regulation of mouse Toll-like receptor 2 gene expression. *J Immunol* 2001;**166**:4516–4524.
34. Gutierrez O, Pipaon C, Inohara N *et al.* Induction of Nod2 in myelomonocytic and intestinal epithelial cells via nuclear factor-κB activation. *J Biol Chem* 2002;**277**:41701–41705.

35. Bowie AG, O'Neill LA. Vitamin C inhibits NF-κB activation by TNF via the activation of p38 mitogen-activated protein kinase. *J Immunol* 2000;**165**: 7180–7188.
36. Ohashi K, Burkart V, Flohe S, Kolb H. Heat shock protein 60 is a putative endogenous ligand of the toll-like receptor-4 complex. *J Immunol* 2000;**164**: 558–561.
37. Roelofs MF, Boelens WC, Joosten LA *et al.* Identification of small heat shock protein B8 (HSP22) as a novel TLR4 ligand and potential involvement in the pathogenesis of rheumatoid arthritis. *J Immunol* 2006;**176**:7021–7027.
38. Okamura Y, Watari M, Jerud ES *et al.* The extra domain A of fibronectin activates Toll-like receptor 4. *J Biol Chem* 2001;**276**:10229–10233.
39. Termeer C, Benedix F, Sleeman J *et al.* Oligosaccharides of hyaluronan activate dendritic cells via toll-like receptor 4. *J Exp Med* 2002;**195**:99–111.
40. Johnson GB, Brunn GJ, Kodaira Y, Platt JL. Receptor-mediated monitoring of tissue well-being via detection of soluble heparan sulfate by Toll-like receptor 4. *J Immunol* 2002;**168**:5233–5239.
41. Schaefer L, Babelova A, Kiss E *et al.* The matrix component biglycan is proinflammatory and signals through Toll-like receptors 4 and 2 in macrophages. *J Clin Invest* 2005;**115**:2223–2233.

Research article

Innate Immunity

14(5) (2008) 298–308
© SAGE Publications 2008
Los Angeles, London,
New Delhi and Singapore
ISSN 1753-4259 (print)
10.1177/1753425908096518

A polymer-type water-soluble peptidoglycan exhibited both Toll-like receptor 2- and NOD2-agonistic activities, resulting in synergistic activation of human monocytic cells

Mizuho Natsuka[1,2], Akiko Uehara[1], Shuhua Yang[1], Seishi Echigo[2], Haruhiko Takada[1]

[1]*Department of Microbiology and Immunology, Tohoku University School of Dentistry, Aoba-ku, Sendai, Japan*
[2]*Department of Oral Surgery, Tohoku University School of Dentistry, Aoba-ku, Sendai, Japan*

Bacterial peptidoglycan (PGN) has been reported to be sensed by cell-surface Toll-like receptor (TLR)2. On the other hand, intracellular NOD-like receptors recognize PGN partial structures: NOD1 and NOD2 recognize the peptide moiety containing diaminopimelic acid, and the muramyldipeptide (MDP) moiety, respectively. In this study, we examined in human monocytic THP-1 cells the pro-inflammatory cytokine-inducing abilities of PGNs and their fragments enzymatically prepared from *Staphylococcus epidermidis* ATCC 155: a polymer-type water-soluble PGN possessing an intact glycan chain (SEPS) and a monomer-type PGN (SEPS-M). The water-soluble PGN polymer, SEPS, exhibited considerably stronger activities to induce pro-inflammatory cytokines than parent PGNs and the PGN monomer, SEPS-M. Short interference RNA targeting TLR2 and NOD2 markedly reduced the activities of SEPS. In the same experiments, the activities of PGNs were mainly reduced in TLR2-silenced cells, whereas the activities of SEPS-M as well as a synthetic MDP were markedly reduced in NOD2-silenced cells. Furthermore, the PGNs and a reference PGN from *Staphylococcus aureus* in combination with MDP synergistically induced interleukin-8 in THP-1 cells. These findings strongly suggested that a polymer-type water-soluble PGN fragment, SEPS, exhibits both TLR2- and NOD2-agonistic activities, which induced the synergistic activation of human monocytic cells.

Keywords: Peptidoglycans, Toll-like receptor (TLR)2, NOD2, human monocytic cells, muramyldipeptide (MDP)

Introduction

Peptidoglycan (PGN) is the back-bone of the cell walls of most bacterial species, and exhibits various biological activities, including immuno-adjuvant activity.[1] Peptidoglycan has a glycan chain composed of β-(1→4)-linked *N*-acetylglucosamine (GlcNAc) and *N*-acetylmuramic acid (MurNAc), which partly carries stem-peptides. Between adjacent stem-peptides, cross-linking occurs sometimes either directly or via an interpeptide bridge, constructing complex reticular heteropolymers as the backbone of cell walls. Schleifer and Kandler[2] proposed taxonomy on the basis of the chemical structures of PGNs. Most Gram-positive bacteria such as *Staphylococcus* spp. and *Streptococcus* spp. have lysine (Lys)-type PGN, in which the third amino acid from MurNAc is L-Lys, which is involved in cross-linking via an interpeptide bridge. On the other hand, most Gram-negative bacteria and some Gram-positive bacteria such as *Mycobacterium* and related bacteria have diaminopimelic acid (DAP)-type PGN, in which the third amino acid is *meso*-DAP, which is involved in direct cross-linking. The minimum structure for the immuno-adjuvant activity of PGN to induce cell-mediated immunity (delayed-type hypersensitivity) against given protein antigens was revealed to be muramyldipeptide (MDP: *N*-acetylmuramyl-L-alanyl-D-isoglutamine).[3,4]

Received 28 January 2008; revised 20 May 2008, 14 July 2008; accepted 17 July 2008

Correspondence to: Akiko Uehara DDS PhD and Haruhiko Takada DDS PhD, Department of Microbiology and Immunology, Tohoku University Graduate School of Dentistry, 4-1 Seiryo-machi, Aoba-ku, Sendai 980-8575, Japan
Tel: +81 22 717-8306; Fax: +81-22-717-8309; E-mail: kyoro@mail.tains.tohoku.ac.jp or dent-ht@mail.tains.tohoku.ac.jp

Chemically synthesized MDP has been demonstrated to exert various biological activities *in vivo* and to activate almost any type of cells so far examined *in vitro*.[5] In 2003, a member of the nucleotide-binding oligomerization domain (NOD) family molecules, NOD2, was demonstrated to be an intracellular receptor for MDP.[6,7] Then, another NOD family molecule, NOD1, was reported to be an intracellular receptor for the DAP-containing peptide moiety of PGN.[8,9]

In humans, nine kinds of Toll-like receptors (TLRs) have been demonstrated as receptors for microbial products.[10] Many reports[11–13] have indicated that PGN is recognized by TLR2, although other reports[14,15] suggested that the TLR2-agonistc activity of PGN should be attributable to minor components contaminating PGN. It must be noted that the activity of MDP is exerted in an TLR2-independent manner.[16,17] Yoshimura *et al.*[18] examined the TLR2-agonistic structure, and found that the purified cell walls of *Staphylococcus epidermidis* ATCC 155, PGNs prepared from the cell walls, and a water-soluble specimen prepared from the PGNs by SALE endopeptidase and designated as SEPS, all of which carry intact glycan chains, exhibited TLR2 agonistic activities. In contrast, a monomer-type PGN fragment prepared by cleaving the glycan chain of SEPS with M-1 endo-*N*-acetylmuramidase and designated as SEPS-M practically lacked TLR2-agonistic activity like synthetic MDP. These findings strongly suggested that the polymer structure carrying the glycan chain is required for PGNs to exert TLR2-agonistic activity. Similar findings with *Staphylococcus aureus* PGNs have been reported by Dziarski and Gupta.[19]

Uehara *et al.*[20] demonstrated that various synthetic TLR-agonists (TLR2-agonistic bacterial lipopeptide, TLR4-agonistic lipid A and TLR9-agonistic bacterial CpG DNA) in combination with synthetic NOD1 or NOD2 ligands induced the synergistic activation of human monocytic THP-1 cells to induce high levels of interleukin (IL)-8. *S. epidermidis* PGNs are Lys-type PGNs, therefore containing MDP moieties. Insoluble PGN might be not transported to intracellular NOD2 molecules, whereas water-soluble SEPS could be transported to NOD2 molecules. Thus, SEPS could exert both TLR2- and NOD2-agonistic activities. If this is true, there is a good possibility that SEPS induces the synergistic activation of cells via both TLR2 and NOD2 pathways. In fact, SEPS is known to exert markedly strong activity as compared with parent PGN and SEPS-M. In this study, to elucidate whether this is true or not, we examined the pro-inflammatory cytokine-inducing activities of SEPS as compared with those of parent PGNs, SEPS-M and related bacterial and synthetic specimens. Further, we examined the possible TLR2 and/or NOD2 usage of these specimens by RNA interference (RNAi) assays targeting the respective genes.

Materials and Methods

PGNs, their fragments and reference materials

The preparation method of purified cell walls and PGNs from *S. epidermidis* ATCC 155 cells were described previously.[21] Briefly, *S. epidermidis* cells were mechanically crushed using glass beads in a Dyno-Mill, type KDL (Willy A, Bichofen Manufacturing Engineers, Basel, Switzerland), and the cell wall fraction was collected and treated with trypsin to purify the cell walls. The purified cell walls were treated with 10% trichloroacetic acid in the cold for 16 h to remove the special structure to prepare PGNs. The preparation method of SEPS and SEPS-M from *S. epidermidis* PGNs, and their chemical analytical data were reported by Kawata *et al.*[22] and Harada *et al.*[23] Briefly, purified PGNs were treated with SALE endopeptidase[22] to cleave the cross-link between stem-peptides, and the water-soluble digests were submitted to gel filtration with connected columns of Sephadex G-50 and G-25. The obtained higher-molecular-mass fraction possessing an intact glycan chain was designated as SEPS, whose chemical structure was assumed on the basis of chemical analytical data as shown in Figure 1. The obtained SEPS was further digested with M-1 endo-*N*-acetylmuramidase[24] to cleave glycan chains, and the digests were again submitted to the above gel filtration to obtain SEPS-M (Fig. 1). The average chain length of the glycan portion was reported to be 10 or 11 disaccharide units with SEPS and 1 unit with SEPS-M.[23] It must be noted that amino acids different from PGNs were scarcely detected in SEPS and SEPS-M, and these preparations were practically endotoxin-free in the *Limulus* test. Reference *S. aureus* PGNs were purchased from Fluka (Buchs, Switzerland). A synthetic MDP and a TLR2/6 agonistic synthetic lipopeptide FSL-1, which mimic the lipopeptide of *Mycoplasma salivarium*, were purchased from the Protein Research Foundation Peptide Institute (Osaka, Japan) and EMC microcollections (Tübingen, Germany), respectively. To rule out possible contamination with lipoprotein(s), SEPS, SEPS-M and reference lipopeptide FSL-1 (each 1 mg/ml) were treated with 50 μg/ml lipoprotein lipase from *Pseudomonas* spp. (Sigma-Aldrich) for 16 h at 37°C according to Hashimoto *et al.*[25]

Cells and cell culture

Human monocytic leukemia cell line THP-1 and U-937 cells, supplied by the Health Science Research Resources Bank (Osaka, Japan), were cultured in RPMI 1640 medium (Nissui Seiyaku, Tokyo, Japan) with 10% heat-inactivated fetal calf serum (JRH, Lenexa, KS,

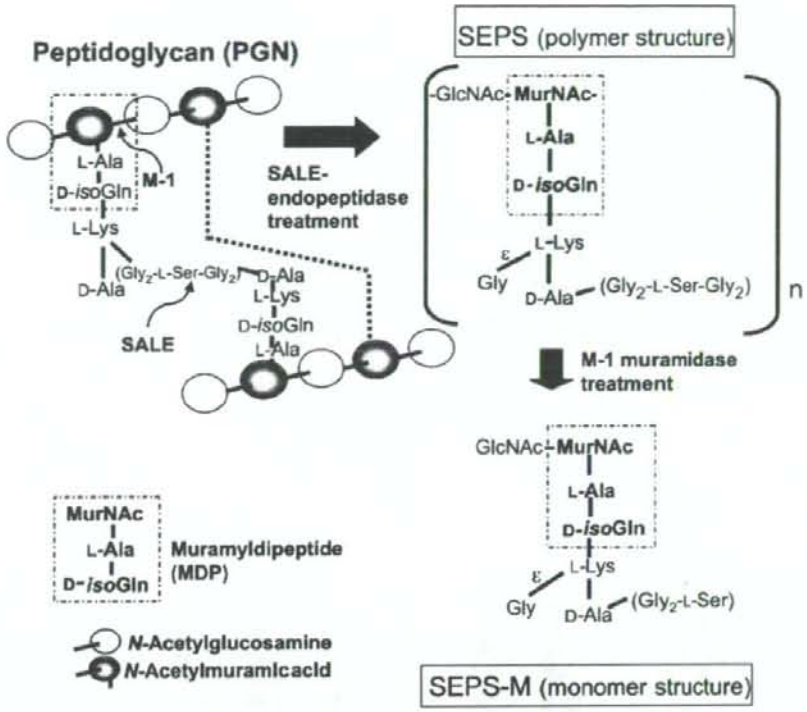

Fig. 1. Schematic preparation procedures and chemical structures of SEPS and SEPS-M from *S. epidermidis* ATCC 155. *S. epidermidis* PGNs were treated with SALE endopeptidase to cleave the cross-link between stem-peptides followed by gel-filtration, and the obtained water-soluble fraction was designated as SEPS, which is a polymer-type PGN fragment carrying the glycan chain. The obtained SEPS was further digested with M-1 endo-*N*-acetylmuramidase to cleave the glycan chain followed by gel filtration, and the obtained monomer-type fragment was designated as SEPS-M.

USA) at 37°C in a humidified CO_2 atmosphere. The cells were maintained in a logarithmic phase of growth (2×10^5 to 2×10^6) by passage every 2–3 days. Cells (2×10^5 cells/ml) were then treated with 0.1 μM 22-oxyacalaitriol (OCT), an analogue of 1α,25-dihydroxy-vitamin D_3, which was supplied by Chugai Pharmaceutical Co. (Tokyo, Japan)[26] for 3 days. The treatment with OCT induced the differentiation of THP-1 and U-937 cells into macrophage-like cells.

Cytokine assay

The cells treated with OCT were collected and washed twice in phosphate-buffered saline (PBS). The cells (1×10^5 cells/ml) were incubated with or without stimulant in RPMI 1640 medium with 1% FCS for 24 h in 96-well flat-bottomed plates (Falcon, Becton Dickinson Labware, Paramus, NJ, USA). After cultivation, the culture supernatants were collected and the levels of cytokines were determined with enzyme-linked immunosorbent assay (ELISA) kits (OptEIA ELISA kits; BD Biosciences; San Diego, CA, USA). The concentration of cytokines in the supernatants were determined using the data analysis program.

RNAi assay

The detailed procedures and characteristics of the obtained transfectants were described previously.[27] Briefly, OCT-1-treated THP-1 cells were collected and washed twice with PBS. After washing, the cells (2×10^6 cells/ml) suspended in 20% FCS-containing Opti-MEM culture medium (Invitrogen; New York, NY, USA) were seeded in 96-well flat-bottomed plates at 50 μl/well. NOD2 short interfering (si) RNA and TLR2 siRNA were diluted with Opti-MEM. In another tube, Lipofectamine 2000 (Invitrogen) was diluted with Opti-MEM, gently mixed, and kept at 20—25°C for 5 min. The diluted

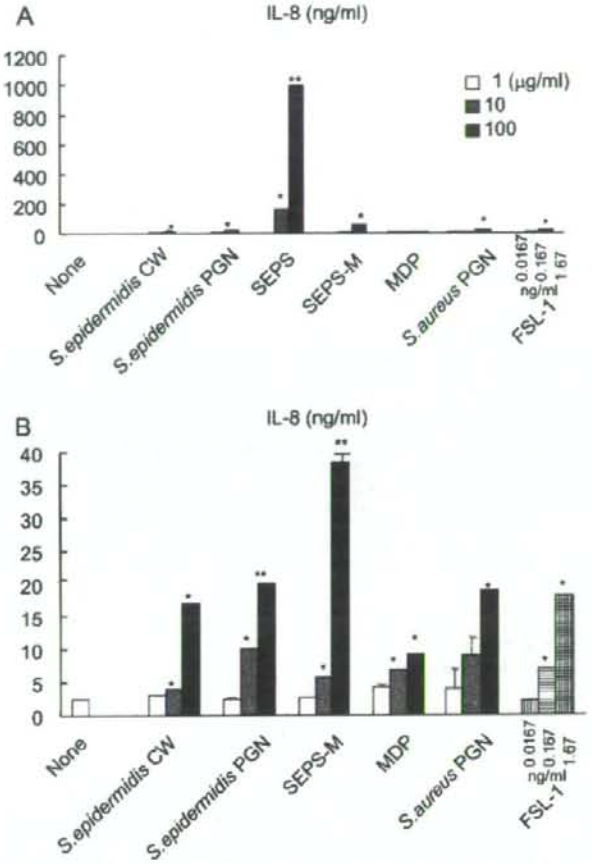

Fig. 2. Induction of IL-8 secretion by *S. epidermidis* PGNs, SEPS, SEPS-M and related specimens in THP-1 cells in culture. The cells treated with OCT were stimulated with cell walls, PGNs, SEPS, SEPS-M prepared from *S. epidermidis*, MDP, *S. aureus* PGNs (1, 10, 100 μg/ml for each specimen) and FSL-1 (0.0167, 0.167, 1.67 ng/ml) for 24 h in triplicate. IL-8 levels in the culture supernatants were determined by ELISA and expressed as mean ± SD (A). Detailed data except SEPS are shown in (B) as an expanded scale, because the activities of other specimens than SEPS were not clearly presented together with that of SEPS. The results are representative of three different experiments. $^{**}P < 0.01$, $^{*}P < 0.05$ versus medium alone.

NOD2 siRNA or TLR2 siRNA was mixed with Lipofectamine 2000, gently mixed, and kept standing for 20 min. This preparation was then added to the above 96-well flat-bottomed plates at 50 μl/well.

Flow cytometry

Flow cytometric analyses were performed using a FACSCalibur flow cytometory and CELLQuest software (BD Biosciences; San Diego, CA, USA). Washed THP-1 cells were stained with mouse monoclonal antibodies specific for TLR2, NOD2 (Santa Cruz), or isotype-matched control IgG at 4°C for 30 min, followed by fluorescein isothiocyanate (FITC)-conjugated anti-mouse IgG (Biosource International; Camarillo, CA, USA) at 4°C for a further 30 min. To calculate the percentage of positive cells, the baseline cursor was set at a channel that yielded less than 2% of the events as positive for the secondary antibody in the absence of the primary antibodies. Fluorescence on the right was counted as specific binding.

Data analysis

All experiments were performed at least three times to confirm reproducibility. For most experiments, the results are shown as the mean ± SD of triplicate assays. The statistical significance of differences between two

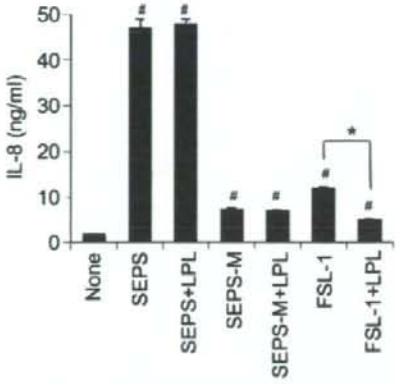

Fig. 3. Treatment with lipoprotein lipase of SEPS and SEPS-M did not influence their activities. Test specimens of SEPS, SEPS-M and reference lipopeptide FSL-1 (each 1 mg/ml) were treated with lipoprotein lipase (LPL, 50 μg/ml), and then SEPS (100 μg/ml), SEPS-M (100 μg/ml) and lipopeptide FSL-1 (1.67 ng/ml), together with the respective untreated materials, were adopted in the IL-8-inducing assay in OCT-treated THP-1 cells for 24 h in triplicate. IL-8 levels in the culture supernatants were determined by ELISA and expressed as mean ± SD. The results are representative of two different experiments. $^{**}P < 0.01$, $^{*}P < 0.05$ versus medium alone.

means was evaluated by one-way analysis of variance (ANOVA), using the Bonferroni or Dunnett method, and *P*-values less than 0.05 were considered significant. In combinatory stimulation experiments, ANOVA of the interaction between test materials was carried out to examine the synergistic effects of the agents.

Results

Water-soluble PGN polymer SEPS induced a high level of IL-8 in THP-1 and U-937 cells

First, human monocytic THP-1 cells pre-treated with OCT were stimulated with *S. epidermidis* cell walls, PGNs, SEPS, SEPS-M, and reference materials; commercial *S. aureus* PGNs, synthetic MDP and FSL-1, and IL-8 in the culture supernatants were determined. Water-soluble PGN SEPS exhibited markedly stronger activity than the other specimens (Fig. 2A), which also showed definite activity, although far less than SEPS (Fig. 2B). To rule out the possibility that the powerful activity of SEPS is attributable to contaminated lipoproteins, we treated SEPS, SEPS-M and the reference lipopeptide FSL-1 with lipoprotein lipase. The IL-8-inducing activities of SEPS and SEPS-M were not influenced by the treatment, whereas the activity of FSL-1 was clearly reduced by the treatment (Fig. 3). It should be noted that the activity of SEPS-M was somewhat weaker than FSL-1 in this experiment. Monocytic U-937 cells pretreated with OCT were also stimulated with these components. As shown in Figure 4, SEPS also exhibited stronger activity than the other specimens, which nevertheless showed significant activity. It must also be noted that the activity of SEPS-M was less than the other specimens in U-937 cells (Fig. 4), while SEPS-M exhibited stronger activity than the other specimens in THP-1 cells (Fig. 2).

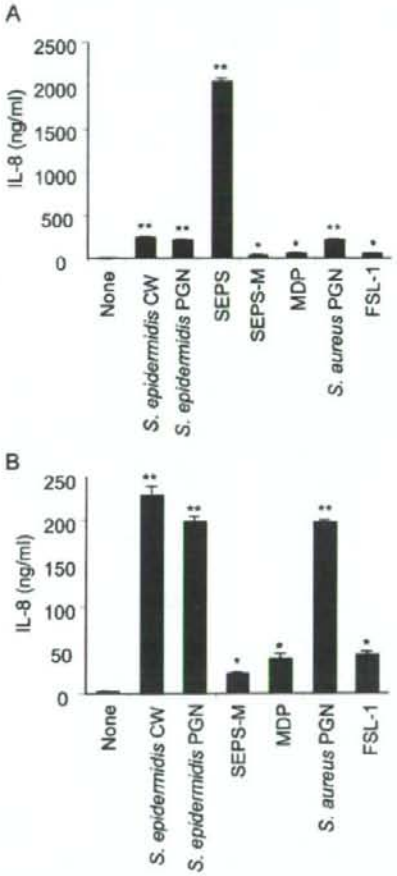

Fig. 4. Induction of IL-8 secretion by *S. epidermidis* PGNs, SEPS, SEPS-M and related specimens in U-937 cells in culture. The cells treated with OCT were stimulated with cell walls, PGNs, SEPS, SEPS-M prepared from *S. epidermidis*, MDP, *S. aureus* PGNs (100 μg/ml for each specimen) and FSL-1 (1.67 ng/ml) at the indicated concentrations for 24 h in triplicate. IL-8 levels in the culture supernatants were determined by ELISA and expressed as mean ± SD (A). Detailed data, except for SEPS, are shown in (B) on an expanded scale, because the activities of specimens other than SEPS were not clear in the presence of SEPS. The results are representative of three different experiments. $^{**}P < 0.01$ versus the respective control.